Revised: CAS-OA-0761-2015; Original article (Cancer Science)

Role of hemoglobin and transferrin in multi-wall carbon nanotube-induced mesothelial injury and carcinogenesis

Yue Wang[1], Yasumasa Okazaki[1], Lei Shi[1], Hiro Kohda[1], Minoru Tanaka[2], Kentaro Taki[2], Tomoki Nishioka[3], Tasuku Hirayama[4], Hideko Nagasawa[4], Yoriko Yamashita[1] and Shinya Toyokuni[1]*

[1]Department of Pathology and Biological Responses, [2]Division for Medical Research Engineering and [3]Department of Cellular Pharmacology, Nagoya University Graduate School of Medicine, 65 Tsurumai-cho, Showa-ku, Nagoya 466-8550, Japan
[4]Laboratory of Pharmaceutical and Medicinal Chemistry, Gifu Pharmaceutical University, 1-25-4 Daigaku-nishi, Gifu 501-1196, Japan

Manuscript: 24 text pages (4,577 words); 7 figures; 2 tables; 2 supplementary figures; 2 supplementary tables
Short running title: Iron in MWCNT-induced mesothelial injury

All correspondence to: *Shinya Toyokuni, M.D., Ph.D.: Department of Pathology and Biological Responses, Nagoya University Graduate School of Medicine, 65 Tsurumai-cho, Showa-ku, Nagoya, Aichi 466-8550, Japan. Tel: +81 52 744 2086; Fax: +81 52 744 2091; E-mail: toyokuni@med.nagoya-u.ac.jp

Keywords:

Multi-wall carbon nanotube, adsorption, mesothelial cell, iron, DNA damage

Abstract

Multi-wall carbon nanotubes (MWCNTs) are flexible fibrous nanomaterial with high electrical and thermal conductivity. However, MWCNT 50 nm in diameter causes malignant mesothelioma (MM) in rodents, and thus the International Agency of Research on Cancer designated them as a possible human carcinogen. The molecular mechanism by which MWCNT causes MM is scarcely known. To elucidate the carcinogenic mechanisms of MWCNT in mesothelial cells, we used a variety of lysates to comprehensively identify proteins specifically adsorbed on pristine MWCNT of different diameters (50 nm, NT50; 100 nm, NT100, 150 nm, NT150 and 15 nm/tangled, NTtngl) using mass spectrometry. We identified >400 proteins, which included hemoglobin, histone, transferrin and various proteins associated with oxidative stress, among which we selected hemoglobin and transferrin for coating MWCNTs to further evaluate cytotoxicity, wound healing, intracellular catalytic ferrous iron and oxidative stress in rat peritoneal mesothelial cells (RPMCs). Cytotoxicity to RPMCs was observed with pristine NT50 but not with NTtngl. Coating NT50 with hemoglobin or transferrin significantly aggravated cytotoxicity to RPMCs, with increase in cellular catalytic ferrous iron and the following DNA damage. Knockdown of transferrin receptor with ferristatin II decreased not only NT50 uptake but also cellular catalytic ferrous iron. Our results suggest that adsorption of hemoglobin and transferrin on the surface of NT50 play a role in causing mesothelial iron overload, contributing to oxidative damage and possibly subsequent carcinogenesis in mesothelial cells. Uptake of NT50 at least partially depends on transferrin receptor. Modifications of NT50 surface may decrease this human risk. (247 words)

Introduction

Carbon nanotubes (CNTs) [1] are a promising material in nanotechnologies due to their high thermal and mechanical resistance but high electrical and thermal conductivity with flexibility and semiconductivity. Thus, CNTs are used worldwide in various industrial and mechanical applications; they are used as components in electronics, energy-storage devices, solar cells and sensors, or as fillers in polymeric composites and concrete [2, 3]. CNTs have also been proposed for use in medicine as nanovectors or as substrates in tissue engineering [4, 5].

Asbestos is natural hydrated silicate fibers. Exposure to asbestos may induce various pathologies in humans, including pleural effusion, pleural plaques and pulmonary asbestosis. Furthermore, this material may cause malignant mesothelioma (MM) and/or lung cancer after a long incubation period [6]. Many rodent experiments support the carcinogenicity of asbestos, especially to mesothelial cells [7-12]. In 2006, at least 40 countries have banned or severely restricted asbestos use [13]. Having a diameter less than 200 nm and a length measured in μm, CNTs have a needle-like shape with a high aspect ratio, which is similar to asbestos. Accordingly, there have been arguments about whether CNTs might have similar carcinogenicity to asbestos. Recently, three independent rodent studies revealed that multi-wall carbon nanotubes (MWCNTs) 50 nm diameter cause MM when injected intraperitoneally to *p53*$^{+/-}$ knockout mice [14] or to wild-type rats [15] or intrascrotally to Fischer-344 rats [16]. In 2014, IARC designated MWCNTs 50 nm in diameter as a possible human carcinogen (Group 2B), based on these studies [17]. Of note, tangled CNTs 15 nm in diameter induce no MM [18] and CNT150 nm are less carcinogenic, which may be partially associated with their difficulty in entering mesothelial cells [15].

Here, we followed our previous strategy for asbestos-induced mesothelial carcinogenesis, which is similar to immunoprecipitation [19, 20], to elucidate the major molecular mechanisms of MWCNT-induced mesothelial carcinogenesis. We used mass spectrometry (MS) to exhaustively identify the proteins that adsorb on the surface of four pristine MWCNTs of different diameters. Among these, we focused on hemoglobin and transferrin, both of which are associated with iron metabolism.

Materials and Methods

Materials and antibodies

Four types of vapor-grown MWCNTs were obtained from Showa Denko (Tokyo, Japan). Characterization of the MWCNTs is summarized in **Table S1**, based on our previous results [15]. Trypsin gold for MS was obtained from Promega (Madison, WI). Albumin from bovine serum (BSA), human holo-transferrin and chlorazol black (ferristatin II) [21] were purchased from Sigma-Aldrich (St. Louis, MO). The Silver Quest staining kit came from Invitrogen (Carlsbad, CA). Antibodies against transferrin (ab1223), transferrin receptor 1 (ab84036), hemoglobin subunit α (ab92492) and peroxiredoxin 6 (ab59543) were purchased from Abcam (Cambridge, MA); Keap1 (D6B12), histone H3 (D1H2), histone H2A (#2578) and histone H2B (#2722) from Cell Signaling Technology (Danvers, MA); hemoglobin β (SC-31116) from Santa Cruz Biotechnology, Inc. (Dallas, TX); and 4-hydroxy-2-nonenal-modified proteins (HNEJ-2) [22] from Nikken Seil Co. Ltd. (Fukuroi, Shizuoka, Japan).

Preparation of tissue lysate

Lung, heart, liver and spleen from eight 24 week-old specific pathogen-free male or female Fischer-344 rats (SLC Japan, Hamamatsu, Japan) were homogenized at 4°C

with lysis buffer (20 mM Tris-HCl, pH 7.4, 0.1% sodium dodecyl sulfate [SDS]) in the presence of protease inhibitors (Complete mini, Roche; Basel, Switzerland), followed by sonication at 4°C for 30 sec. After centrifugation (15000 x g) at 4°C for 10 min, the protein concentration was measured with a Protein Assay Bicinchninate Kit (Nacalai Tesque, Kyoto, Japan). Animal experiment committee of Nagoya University Graduate School of Medicine approved this experiment.

Preparation of MWCNT suspension and hemoglobin- or holo-transferrin-coated MWCNTs

MWCNTs were suspended in 10 mM phosphate-buffered saline, pH 7.4 (D-PBS[-], Wako) containing 0.5% BSA, and then sonicated at 4°C for 2 h to 5 mg/ml. As preparation of hemoglobin- or holo-transferrin-coated MWCNTs, an amount of 400 μg of hemoglobin or holo-transferrin protein was added to 20 μl of 5 mg/ml MWCNTs suspension. PBS containing 0.5% BSA was added up to 1 ml, followed by 3 h-incubation at 37°C. The mixture was centrifuged at 20,000 x g for 2 min, and the supernatant was discarded. The pellet was washed three times with PBS containing 0.5% BSA. All samples were prepared immediately before use.

Protein adsorption on MWCNTs

Immunoprecipitation-like assay (CNT immunoprecipitation) was performed as described [19, 20]. Briefly, lysate (400 μg) and MWCNT (250 μg) were mixed, and PBS was added up to 1 ml. Crocidolite (UICC; Geneva, Switzerland) was used as a positive control. After 3 h-incubation at 37°C, the mixture was centrifuged (15,000 × g) at 4°C for 10 min. The pellets were washed 5 times with PBS. SDS-polyacrylamide gel electrophoresis (SDS-PAGE) sample buffer was added, and the samples were boiled for 10 min. The samples were then centrifuged (15,000 × g)

at 4°C for 5 min, and the supernatants were evaluated with SDS-PAGE. The gel was stained with a silver staining kit.

Assessment of MWCNTs adsorption ability

To calculate the amount of proteins adsorbed on the surfaces of the MWCNTs, the concentration of proteins remaining in the supernatant was measured using a spectrophotometer (NanoDrop 2000, Thermo Fisher Scientific; Waltham, MA), which was deducted from the control value.

Identification of proteins adsorbed on MWCNT with LC/MS/MS

Mass spectrometric identification of the proteins was performed as described [19, 23]. Briefly, for in-gel digestion, proteins run on SDS-PAGE were visualized with silver staining; each band was excised from the gels and subjected to in-gel digestion with trypsin in a buffer containing 25 mM ammonium bicarbonate overnight at 37°C. For in-solution digestion, the proteins were detached from MWCNTs by degeneration with guanidinium chloride and digested with trypsin in the same manner. Molecular mass analysis of the tryptic peptides was performed with an LTQ Orbitrap XL (Thermo Fisher Scientific). Proteins were identified by LC/MS/MS, and theoretical peptide masses from the proteins were registered in Swiss-Prot. The experiments were performed in triplicate.

Western Blotting

This was performed as previously described [24].

Cell Culture

Rat peritoneal mesothelial cells (RPMCs) were produced as described [25, 26], plated at

a density of 3 × 10^4 cells/cm^2 and incubated for 24 h. RPMCs were cultured in RPMI-1640 medium (189-02025, Wako) with 10% fetal bovine serum (Biowest, Nuaillé, France) and 1% Antibiotic-Antimycotic (15240-062, Invitrogen). RPMCs were maintained in a humidified incubator at 37°C with 5% CO_2, as described [27].

MWCNT cytotoxicity Assay

RPMCs were plated at a density of 3 × 10^4 cells/cm^2 and incubated for 24 h before adding MWCNTs. MWCNTs were added to RPMCs to a final concentration of 10 μg/cm^2. After 72 h incubation, dead-cell protease activity assay (CytoTox-Glo Cytotoxicity Assay, Promega) was used to measure the cytotoxicity.

Wound-healing Assay

RPMCs were plated at a density of 3 × 10^4 cells/cm^2 and incubated to confluence. RPMCs were given a straight scratch with a pipette, followed by washing 3 times with PBS. MWCNTs were added to RPMCs at a final concentration of 10 μg/cm^2. The same procedure, without adding the MWCNTs, was performed as a control. Pictures were taken 0, 8 and 24 h later with the optical microscope. The wounded area was evaluated with ImageJ (imagej.nih.gov/ij/).

Visualization of intracellular catalytic ferrous ion (Fe[II]).

RhoNox-1 (10 μM, 30-min incubation at 37 °C) was used as described [28, 29]. RPMCs were plated at a density of 3 × 10^4 cells/cm^2 and incubated for 24 h before adding MWCNTs to a final concentration of 10 μg/cm^2. As a control, medium was added. After 24 h incubation, the cells were stained and observed with a fluorescent microscope (BZ-9000; Keyence Corporation; Osaka, Japan).

Lipid peroxidation assay

We evaluated lipid peroxidation, using an antibody against 4-hydroxy-2-nonenal (HNE) and BODIPY (581/591) C_{11} as the lipid peroxidation sensor probe (Thermo Fisher). RPMCs were plated at a density of 3×10^4 cells/cm^2 and incubated for 24 h before adding MWCNTs to a final concentration of 10 μg/cm^2. For Western blot analysis, after treating cells with MWCNTs for 24 h, the cells were collected and lysed with RIPA buffer. For BODIPY (581/591) C_{11}, after treating cells with MWCNTs for 24 h, BODIPY C_{11} (final concentration 5 μM) was added to 5×10^6 cells per ml, incubated for 15 min at room temperature, and washed twice (200 × *g* for 5 min), which was analyzed with a Gallios flow cytometer (Beckman Coulter, Brea, CA).

Comet assay

Alkaline comet assay was performed according to the method of Dhawan A. *et al* [30] with modifications. Approximately 8,000 cells in 10 μl or less volume were mixed with 50 μl of low melting point agarose and layered on the CometSlide (CommetAssay; Trevigen, Gaithersburg, MD). After preparation, the slide was immersed in lysis solution and refrigerated at 4°C for 2 h. After lysis, the slide was placed in alkaline electrophoresis buffer for 30 min to allow salt equilibration and further DNA unwinding. Electrophoresis was performed at 300 mA for 30 min at 4°C. The slide was then washed 3 times with neutralization buffer for 10 min. The cells were stained with 50 μl of ethidium bromide. Comet images were taken with a fluorescent microscope. The tail moment of the DNA was analyzed using an image analysis system (casplab.com) [31], and the tail length was scored by direct measurements. A total of 50 cells were analyzed per sample for quantitation.

Apoptosis assay

TACS annexin V kit (Trevigen, Gaithersburg, MD) was used according to the protocol provided in the kits. The stained cells were analyzed using a Gallios flow cytometer.

Ferristatin II treatment to downregulate the transferrin receptor

RPMCs were plated at a density of 3×10^4 cells/cm^2. After 24 h of incubation, cells were washed three times with PBS containing 1 mM $MgCl_2$ and 0.1 mM $CaCl_2$ (PBS++) and then washed once with serum-free medium. After adding 50 μM ferristatin II or dimethyl sulfoxide as a vehicle control to the RPMCs in serum-free medium, the cells were incubated at 37°C with 5% CO_2 for 4 h, as described [21].

Measurements of MWCNTs in cells

We added MWCNTs to the ferristatin II-treated or non-treated RPMCs at a concentration of 10 μg/cm^2. After 24 h of incubation, the amounts of MWCNTs taken up by cells were calculated by flow cytometry, as described [32, 33].

Statistical analysis

A two-way ANOVA, a one-way ANOVA or an unpaired Student's *t*-test was applied. $P<0.05$ was considered statistically significant.

Results

Proteins adsorbed on the surface of MWCNTs

We named the MWCNTs NT50, NT100, NT150 and NTtngl, according to their average diameter, as described [15]. **Figure 1** shows a variety of proteins after CNT

precipitation and gel electrophoresis followed by silver staining. Regarding the lung lysate, the banding pattern of each CNT showed a similar pattern, including crocidolite. NT50 revealed the highest adsorption with the highest number of protein bands (**Fig. 1A**). However, the banding patterns were different between NT50 and NTtngl when heart, liver and spleen were analyzed (**Fig. 1B-D**). Each protein's affinity to each CNT was distinct.

Identification of proteins with mass spectrometry

To exhaustively identify proteins adsorbed on MWCNTs, we undertook both in-solution and in-gel digestion methods. With the in-solution digestion method, we identified 321 proteins from NT50, 131 proteins from NT100, 231 proteins from NT150 and 287 proteins from NTtngl (**Table 1** and **Table S2**). The results of the in-solution digestion method revealed that NT50 and NTtngl shared the highest number of proteins among the four MWCNTs (**Fig. 2A**). More than 400 proteins were identified and classified (**Table S2**). These included histones and many proteins associated with iron metabolism or oxidative stress. We picked up histones 2A/2B/3, hemoglobin α chain, hemoglobin β chain, Keap1, transferrin and peroxiredoxin 6 for confirmation (**Fig. 2B**). For histones, each of the four CNT fiber types revealed similar affinities (**Fig. 2Ba**). However, for the other proteins studied, NT50 and NTtngl adsorbed significantly larger amounts of the proteins investigated than did NT100, NT150 or crocidolite, with similar affinities, except for transferrin (**Fig. 2Bb**). Generally, the results were proportional to the surface area of each CNT (**Fig. S1**). NT50, which is potently carcinogenic to mesothelial cells, showed a higher affinity for transferrin than NTtngl, which shows no carcinogenicity to mesothelial cells [(18)].

Protein coating increased the cytotoxicity of MWCNTs

We evaluated the cytotoxicity of MWCNTs to RPMCs with dead-cell protease activity assay (**Fig. 3A**). The RPMCs were exposed to pristine CNT (Nt-NT50) or CNT after incubation with hemoglobin (Hb-NT50), holo-transferrin (Tf-NT50), or lung lysate (Lys-NT50). NT50 and NTtngl were used as carcinogenic and non-carcinogenic CNTs, respectively. The cells treated with Nt (non-treated)-NT50 showed ~1.4-fold dead cells, and Hb-NT50 and Tf-NT50 revealed ~1.8- and ~1.9-fold dead cells, respectively, compared with the untreated control. Lys-NT50 induced the most dead cells with an ~2.3-fold increase. In contrast, neither pristine NTtngl (Nt-NTtngl) nor NTtngl after incubation with Hb (Hb-NTtngl) or Tf (Tf-NTtngl) showed cytotoxicity to RPMCs. We also performed a wound-healing assay to evaluate the proliferation of RPMCs (**Fig. 3BC**). Nt-NT50 and Tf-NT50 decreased the proliferation of cells by ~10%. However, Hb-NT50 and Lys-NT50 caused 24% and 31% decreases, respectively.

Hemoglobin- or holo-transferrin-coated NT50 increased intracellular catalytic Fe(II) in association with lipid peroxidation

RhoNox-1 was used to visualize catalytic (labile) Fe(II). We confirmed that neither hemoglobin nor holo-transferrin increase the fluorescence intensity of RhoNox-1 **(Fig. S2)**. After treatment with Hb-NT50 or Tf-NT50, catalytic Fe(II) in cells increased more significantly than in the cells treated with Nt-NT50 (**Fig. 4A**). In contrast, neither Hb-NTtngl, Tf-NTtngl, nor Nt-NTtngl affected the intracellular catalytic Fe(II). To assess whether increased catalytic Fe(II) induces oxidative stress in cells, lipid peroxidation products, 4-hydroxy-2-nonenal (HNE)-modified proteins [(22)] were measured as a marker of oxidative stress by Western blot with a monoclonal antibody **(Fig. 4B)** and flow cytometry was used with a lipid peroxidation sensor

probe BODIPY (581/591) C_{11} **(Fig. 4C).** Treatment with Nt-NT50 significantly increased lipid peroxidation, which was aggravated with the use of Tf-NT50 or Lys-NT50.

Hemoglobin- or holo-transferrin-treated NT50 increased DNA damage

We used RPMCs exposed to hemoglobin- or holo-transferrin-treated NT50 for comet assay. Two measures, tail length (length of DNA fragment) and tail moment (amount of DNA fragment in tail), were used to evaluate the DNA damage. Whereas no significant increase in tail length or tail moment was observed with Nt-NT50, coating with Hb, Tf or lung lysate significantly increased these measures **(Fig. 5A-C)**. Notably, we observed an increase in dead cells, presumably via apoptosis, only in Lys-NT50 (**Fig. 5D**).

Transferrin receptor plays a role in the uptake of Tf-NT50

After treating RPMCs with Nt-NT50 or Lys-NT50, we observed a difference in uptake, suggesting that an interaction between nanotube surface protein and its receptor may promote NT50 internalization (**Fig. 6A**). To evaluate whether NT50 uptake was associated with the plasma membrane receptor for Tf, flow cytometric analysis was performed [33] to calculate the number of cells revealing NT50 uptake by counting 10,000 cells. Tf-NT50 induced ~20% more uptake of CNTs by RPMC than Nt-NT50 (**Fig. 6B**). TfR1 is the main receptor of transferrin. Ferristatin II is a specific inhibitor of TfR1, and the ferristatin II-induced decrease in TfR1 protein levels was confirmed with Western blot analysis (**Fig. 6C**). Ferristatin II significantly decreased the amount of Tf-NT50 penetrating the cells (**Fig. 6D**). Simultaneously, the level of catalytic ferrous iron was also decreased in Tf-NT50-treated cells after ferristatin II addition (**Fig. 6E**).

Discussion

Risk assessment of CNTs is important because CNTs are already in the market due to their superb utility as an industrial material [2, 3]. We previously observed that carcinogenic NT50 was likely to enter mesothelial cells, probably via penetration [34]. Based on our previous asbestos studies, we used lysates from various rat organs including lung, which is a putative major target for exposure in humans. Here we identified >400 proteins adsorbed on these CNTs (**Table 1 and Table S2**). The 104 adsorptive proteins, common to all four of the MWCNTs tested, included hemoglobin (Hb), transferrin (Tf), histones, DNA helicase, actin and tubulin. Of note, asbestos did not adsorb Tf in our previous experiments [19], but all of the other proteins above were in common with asbestos. Many proteins were associated with oxidative stress in the current experiments on MWCNT, which included Keap1, cytochrome P450, aldehyde dehydrogenase, thioredoxin, glutathione *S*-transferase, heat shock protein, peroxiredoxin and proteasome (**Table S2**).

Among those proteins, we decided to focus on Hb and Tf, considering not only the result that only CNTs, especially NT50, adsorbed Tf but also a close association between excess iron and carcinogenesis [35]. Approximately 60% of the iron is present in the heme of Hb in erythrocytes. Due to its richness in capillaries, lung tissue contains a large amount of Hb.

Coating NT50 with Hb or Tf significantly increased mesothelial damage (**Fig. 3A**) and significantly delayed wound healing with Hb or lung lysate (**Fig. 3BC**); a similar effect was not observed with NTtngl, likely because NTtngl does not enter mesothelial cells [15]. We evaluated the effects of NT50 coated with Hb and Tf from the viewpoint of catalytic Fe(II) and lipid peroxidation. Catalytic Fe(II) can initiate

Fenton reaction that generates hydroxyl radicals to start lipid peroxidation [36, 37]. Hb and Tf coating significantly increased the catalytic Fe(II) in RPMCs detected with RhoNox-1 [29] and HNE-modified proteins [38] simultaneously (**Fig. 4**), suggesting that NT50 exposure induces high levels of oxidative stress in mesothelial cells. This was also supported by an observation of increased intracellular Tf itself with Western blot analysis (data not shown).

Then, we evaluated whether oxidative stress can cause DNA damage with comet assay and found that only Hb- or Tf-coated NT50 induced DNA strand breaks in mesothelial cells, whereas pristine NT50 did not (**Fig. 5AB**). Mesothelial damage with less cellular death in the case of Hb or Tf coating (**Fig. 5D**) might contribute to more mutations in mesothelial cells through NT50. We interpret here that Hb- or Tf-coated NT50 can induce various kinds of DNA damage including DNA double-strand breaks. Thus, further studies are necessary to identify and quantify precise DNA lesions.

In the previous carcinogenesis experiments, we observed iron accumulation in areas near CNT deposits [15]. Excess iron has been associated with DNA strand breaks [39, 40], which may lead to homozygous deletion of *Cdkn2A/2B* as observed in Fenton reaction-induced renal carcinogenesis in rats [41, 42]. Reportedly, iron overload is a major pathogenesis in asbestos-induced mesothelial carcinogenesis, including the case of chrysotile containing no iron *per se*, where hemolysis followed by surface Hb adsorption, induces similar pathology of iron overload [11]. Together with our previous finding of a high incidence of homozygous deletion of *Cdkn2A/2B* in CNT-induced mesothelial carcinogenesis [15], these new results strongly support the hypothesis that excess iron possibly derived from Hb and Tf plays a role in the molecular mechanism of NT50-induced mesothelial carcinogenesis.

Finally, we evaluated the role of Tf receptor 1, based on the result that coating

NT50 with lung lysate or Tf significantly increased the uptake of NT50 by RPMCs (**Fig. 6AB**). Decreasing Tf receptor 1 with ferristatin II significantly decreased NT50 uptake and cytoplasmic catalytic Fe(II) (**Fig. 6C-E**). These findings demonstrate, for the first time, the involvement of Tf and its receptor in the NT50 uptake by mesothelial cells, in addition to simple penetration, which provided a new molecular mechanism of MWCNTs in mesothelial cell damage. Surprisingly, 18% decrease in the uptake of NT50 dramatically changed intracellular catalytic Fe(II). This may be associated with iron metabolism in mesothelial cells, especially storage and export, which needs further investigation.

In conclusion, our results suggest that adsorptive activity of NT50 for proteins, especially hemoglobin and transferrin, is a major mechanism in mesothelial damage followed by carcinogenesis. It works for the efficient NT50 uptake by mesothelial cells and also for the increased catalytic Fe(II), leading to DNA damage **(Fig. 7)**. Therefore, chemical modification of CNT to avoid Hb and Tf adsorption might decrease the human risk to CNT-induced mesothelial carcinogenesis. Many more adsorptive proteins on MWCNTs await evaluation.

Acknowledgments

This work was supported, in part, by the National Cancer Center Research and Development Fund (25-A-5), a Grant-in-aid for research from the Ministry of Education, Culture, Sports, Science and Technology (MEXT) of Japan (24390094; 221S0001-04; 24108001) and the Yasuda Medical Foundation. The authors wish to thank Nobuaki Misawa for excellent technical assistance with the pathologic specimens.

Disclosure Statement

The authors declare that they have no competing interests.

Figure legends

Fig. 1. Adsorption of specific proteins on multi-wall carbon nanotubes (MWCNT). Lysates from (A) lung, (B) heart, (C) liver, or (D) spleen were incubated with MWCNTs of four distinct diameters (NT50, NT100, NT150 and NTtngl; 50, 100, 150 and 15 nm [tangled], respectively), washed and analyzed by sodium dodecyl sulfate polyacrylamide gel electrophoresis (SDS-PAGE) followed by silver staining. The original band patterns of the lysates are shown for comparison. Notably, each MWCNT showed specific adsorption. NT50 revealed the highest protein adsorption with a higher number of protein bands. The numbers with red arrows correspond to those in **Table 2**, in which the in-gel digestion method was used for protein identification. Please refer to the text for details. Cro, crocidolite.

Fig. 2. Analysis of adsorbed proteins identified with mass spectrometry.
Proteins adsorbed on the surface of each MWCNT were identified with liquid chromatography/mass spectrometry/mass spectrometry (LC/MS/MS). The results from each sample were compared for overlap (A). Three histones (H2A, H2B and H3), two subunits of hemoglobin (Hb-α and Hb–β) and three other proteins (Tf, transferrin; Prdx6, peroxiredoxin 6) associated with oxidative stress and based on our previous experiments on asbestos were picked from the common cluster and were confirmed with Western blotting analysis (B). Please refer to the text for details.

Fig. 3. Hemoglobin- or holo-transferrin-coating increase the cytotoxicity of MWCNTs to rat peritoneal mesothelial cells (RPMCs).
A study of cell viability in RPMCs after a 72-h incubation with protein-coated NT50 (coated with hemoglobin, Hb-NT50; coated with transferrin, Tf-NT50; coated with

lung lysate, Lys-NT50) at 10 μg/cm^2 revealed higher cytotoxicity than pristine non-treated NT50 (Nt-NT50). This effect was not observed in NTtngl, even after the same coating procedures (A). Wound healing assays showed that hemoglobin or lung lysate coating retarded cellular proliferation compared to Nt-NT50 (B and C) (N = 3, means ± SEM; * P < 0.05, ** P < 0.01, *** P < 0.005, ****P < 0.001).

Fig. 4. Take-up of hemoglobin- or transferrin-coatedNT50 by RPMCs increases the intracellular catalytic Fe(II).

After incubating RPMCs with hemoglobin- or transferrin-coatedNT50 (a-d) or NTtngl with the same coatings (e-h), the cells were stained with a fluorescent probe (Rhonox-1) that is highly specific to catalytic Fe(II) (A). Intracellular catalytic Fe(II) was significantly increased only in the case of hemoglobin- or transferrin-coatedNT50, but not NTtngl. The levels of lipid peroxidation were evaluated with an antibody against 4-hydroxy-2-nonenal (HNE)-modified proteins (B), and lipid peroxidation sensor probe BODIPY (581/591) C_{11} (C), which were consistent with the amounts of catalytic Fe(II) (N = 3, means ± SEM; * P < 0.05, ** P < 0.01, *** P < 0.005, ****P < 0.001).

Fig. 5. Hemoglobin- or holo-transferrin-coating of MWCNTs induces DNA damage to RPMCs without causing apoptosis.

We used a comet assay to determine whether protein coating may cause DNA damage in RPMCs. Tail length (A). Tail moment (B). Examples of scoring in comet assay (C). We observed a significant increase in dead cells, presumably through apoptosis, only when lung lysate was used to coat NT50 after 4 h or 8 h of incubation (D and E; * P < 0.05, ** P < 0.01, *** P < 0.005, ****P < 0.001).

Fig. 6. Transferrin receptor plays a role in the uptake of NT50 by RPMCs.

Difference in the uptake of NT50 by RPMCs with (b, Lys-NT50) or without (a, Nt-NT50) protein coating (A). The amount of Nt-NT50 or Tf-NT50 around or intenalization was measured by flow cytometer (B). Ferristatin II reduced the number of transferrin receptors (C), which induced decreased uptake of Tf-NT50 (D). Whereas ferristatin II treatment alone did not change the level cytoplasmic catalytic Fe(II), ferristatin II treatment significantly decreased the amounts of catalytic Fe(II) upon exposure to Tf-NT50 (N = 3, means ± SEM; * $P < 0.05$, ** $P < 0.01$, *** $P < 0.005$, ****$P < 0.001$). Please refer to the text and Fig. 4 for details.

Fig. 7. Role of hemoglobin and transferrin in MWCNT-induced mesothelial injury and carcinogenesis. Adsorption of hemoglobin and transferrin on MWCNT provides another molecular mechanism to injure mesothelial cells, which is distinct from direct physical injury such as piercing.

List of supplementary files

Fig. S1 (Supplementary Fig. 1). Amounts of adsorbed protein.

Fig. S2 (Supplementary Fig. 2). Neither hemoglobin nor transferrin increases the fluorescence intensity of RhoNox-1.

Table S1 (Supplementary Table 1) Summary table of characteristics of MWCNTs.

Table S2 (Supplementary Table 1) The list of In-solution digestion results.

Abbreviations

CNT, carbon nanotube

Hb, hemoglobin

IARC, International Agency of Research on Cancer

LC/MS/MS, liquid chromatography/mass spectrometry/mass spectrometry

MWCNT, multi-wall carbon nanotube

PBS, phosphate-buffered saline

PVDF, polyvinylidene fluoride

RPMC, rat peritoneal mesothelial cell

SDS-PAGE, sodium dodecyl sulfate-polyacrylamide gel electrophoresis

Tf, transferrin

References

1 Iijima S. Helical Microtubules of Graphitic Carbon. *Nature* 1991; **354**: 56-8.

2 Endo M, Strano MS, Ajayan PM. Potential applications of carbon nanotubes. Carbon nanotubes: Springer, 2008; 13-62.

3 Lee J, Mahendra S, Alvarez PJJ. Nanomaterials in the construction industry: a review of their applications and environmental health and safety considerations. *ACS Nano* 2010; **4**: 3580-90.

4 Liu Z, Tabakman S, Welsher K, Dai H. Carbon nanotubes in biology and medicine: in vitro and in vivo detection, imaging and drug delivery. *Nano Res* 2009; **2**: 85-120.

5 Zhang Y, Bai Y, Yan B. Functionalized carbon nanotubes for potential medicinal applications. *Drug Discov Today* 2010; **15**: 428-35.

6 Kamp DW. Asbestos-induced lung diseases: an update. *Transl Res* 2009; **153**: 143-52.

7 Wagner J, Berry G, Skidmore J, Timbrell V. The effects of the inhalation of asbestos in rats. *Br J Cancer* 1974; **29**: p252-69.

8 Bolton R, Davis J, Donaldson K, Wright A. Variations in the carcinogenicity of mineral fibres. *Ann Occup Hyg* 1982; **26**: p569-82.

9 Whitaker D, Shilkin K, Walters M. Cytologic and tissue culture characteristics of asbestos-induced mesothelioma in rats. *Acta Cytol* 1984; **28**: p185-9.

10 Suzuki Y, Kohyama N. Malignant mesothelioma induced by asbestos and zeolite in the mouse peritoneal cavity. *Environ Res* 1984; **35**: 277-92.

11 Jiang L, Akatsuka S, Nagai H, *et al.* Iron overload signature in chrysotile-induced malignant mesothelioma. *J Pathol* 2012; **228**: 366-77.

12 Aierken D, Okazaki Y, Chew SH, *et al.* Rat model demostrates a high risk of tremolite but a low risk of anthophyllite for mesothelial carcinogenesis. *Nagoya J Med Sci* 2014; **76**: 149-60.

13 Wagner GR. The fallout from asbestos. *Lancet* 2007; **369**: 973-4.

14 Takagi A, Hirose A, Nishimura T, et al. Induction of mesothelioma in p53+/- mouse by intraperitoneal application of multi-wall carbon nanotube. *J Toxicol Sci* 2008; **33**: p105-16.

15 Nagai H, Okazaki Y, Chew S, *et al.* Diameter of multi-walled carbon nanotubes is a critical factor in mesothelial injury and subsequent carcinogenesis. *Proc Natl Acad Sci U S A* 2011; **108**: E1330-8.

16 Sakamoto Y, Nakae D, Fukumori N, *et al.* Induction of mesothelioma by a single intrascrotal administration of multi-wall carbon nanotube in intact male Fischer 344 rats. *J Toxicol Sci* 2009; **34**: 65-76.

17 Grosse Y, Loomis D, Guyton KZ, *et al.* Carcinogenicity of fluoro-edenite, silicon carbide fibres and whiskers, and carbon nanotubes. *Lancet Oncol* 2014; **15**: 1427-8.

18 Nagai H, Okazaki Y, Chew SH, *et al.* Intraperitoneal administration of tangled multiwalled carbon nanotubes of 15 nm in diameter does not induce mesothelial carcinogenesis in rats. *Pathol Int* 2013; **63**: 457-62.

19 Nagai H, Ishihara T, Lee WH, *et al.* Asbestos surface provides a niche for oxidative modification. *Cancer Sci* 2011; **102**: 2118-25.

20 Kubo Y, Takenaka H, Nagai H, Toyokuni S. Distinct affinity of nuclear proteins to the surface of chrysotile and crocidolite. *J Clin Biochem Nutr* 2012; **51**: 221-6.

21 Byrne SL, Buckett PD, Kim J, *et al.* Ferristatin II promotes degradation of transferrin receptor-1 in vitro and in vivo. *PLoS ONE* 2013; **8**: e70199.

22 Toyokuni S, Miyake N, Hiai H, *et al.* The monoclonal antibody specific for the 4-hydroxy-2-nonenal histidine adduct. *FEBS Lett* 1995; **359**: 189-91.

23 Yamashita K, Nagai H, Toyokuni S. Receptor role of annexin A2 in the mesothelial endocytosis of crocidolite fibers. *Lab Invest* 2015; **95**: 749-64.

24 Toyokuni S, Kawaguchi W, Akatsuka S, Hiroyasu M, Hiai H. Intermittent microwave

irradiation facilitates antigen-antibody reaction in Western blot analysis. *Pathol Int* 2003; **53**: 259-61.

25 Yamashita Y, Tsurumi T, Mori N, Kiyono T. Immortalization of Epstein-Barr virus-negative human B lymphocytes with minimal chromosomal instability. *Pathol Int* 2006; **56**: 659-67.

26 Jiang L, Yamashita Y, Toyokuni S. A novel method for efficient collection of normal mesothelial cells *in vivo*. *J Clin Biochem Nutr* 2010; **46**: 265-8.

27 Jiang L, Yamashita Y, Chew SH, *et al.* Connective tissue growth factor and β-catenin constitute an autocrine loop for activation in rat sarcomatoid mesothelioma. *J Pathol* 2014; **233**: 402-14.

28 Hirayama T, Okuda K, Nagasawa H. A highly selective turn-on fluorescent probe fro iron(II) to visualize labile iron in living cells. *Chem Sci* 2013; **4**: 1250-6.

29 Mukaide T, Hattori Y, Misawa N, *et al.* Histological detection of catalytic ferrous iron with the selective turn-on fluorescent probe RhoNox-1 in a Fenton reaction-based rat renal carcinogenesis model. *Free Radic Res* 2014; **48**: 402-14.

30 Dhawan A, Bajpayee MM, Pandey AK, Parmar D. Protocol for the single cell gel electrophoresis/comet assay for rapid genotoxicity assessment. *Sigma* 2003; **1077**: 1.

31 Końca K, Lankoff A, Banasik A, *et al.* A cross-platform public domain PC image-analysis program for the comet assay. *Mutat Res/Genet Toxicol Environ Mutag* 2003; **534**: 15-20.

32 Al-Jamal KT, Kostarelos K. Assessment of cellular uptake and cytotoxicity of carbon nanotubes using flow cytometry. Carbon Nanotubes: Springer, 2010; 123-34.

33 Yamashita K, Nagai H, Kondo Y, Misawa N, Toyokuni S. Evaluation of two distinct methods to quantify the uptake of crocidolite fibers by mesothelial cells. *J Clin Biochem Nutr* 2013; **53**: 27-35.

34 Nagai H, Toyokuni S. Differences and similarities between carbon nanotubes and

asbestos fibers during mesothelila carcinogenesis. *Cancer Sci* 2012; **103**: 1378-90.

35 Toyokuni S. Role of iron in carcinogenesis: Cancer as a ferrotoxic disease. *Cancer Sci* 2009; **100**: 9-16.

36 Toyokuni S. Reactive oxygen species-induced molecular damage and its applicaton in pathology. *Pathol Int* 1999; **49**: 91-102.

37 Toyokuni S. Iron and thiols as two major players in carcinogenesis: friends or foes? *Front Pharmacol* 2014; **5**.

38 Toyokuni S, Uchida K, Okamoto K, Hattori-Nakakuki Y, Hiai H, Stadtman ER. Formation of 4-hydroxy-2-nonenal-modified proteins in the renal proximal tubules of rats treated with a renal carcinogen, ferric nitrilotriacetate. *Proc Natl Acad Sci USA* 1994; **91**: 2616-20.

39 Toyokuni S, Sagripanti J-L. DNA single- and double-strand breaks produced by ferric nitrilotriacetate in relation to renal tubular carcinogenesis. *Carcinogenesis* 1993; **14**: 223-7.

40 Toyokuni S, Sagripanti J-L. Association between 8-hydroxy-2'-deoxyguanosine formation and DNA strand breaks mediated by copper and iron. *Free Radic Biol Med* 1996; **20**: 859-64.

41 Toyokuni S. Mysterious link between iron overload and CDKN2A/2B. *J Clin Biochem Nutr* 2011; **48**: 46-9.

42 Akatsuka S, Yamashita Y, Ohara H, *et al.* Fenton reaction induced cancer in wild type rats recapitulates genomic alterations observed in human cancer. *PLoS ONE*. 2012; **7**: e43403.

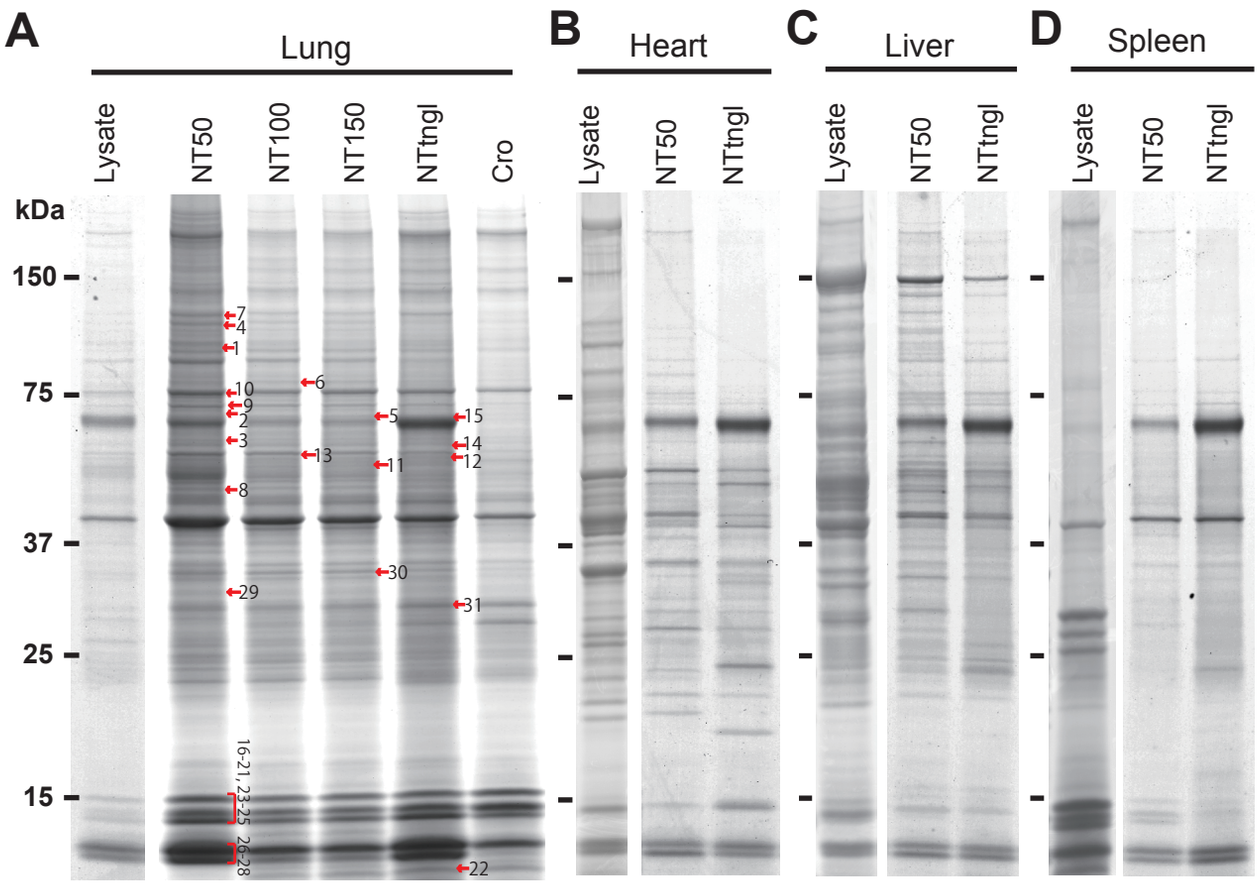
A
Lung
B
Heart
C
Liver
D
Spleen
Lysate
NT50
NT100
NT150
NTtngl
Cro
kDa
150
75
37
25
15
7
4
1
10
9
2
3
8
29
6
13
5
11
30
15
14
12
31
16-21, 23-25, 26-28
22

A

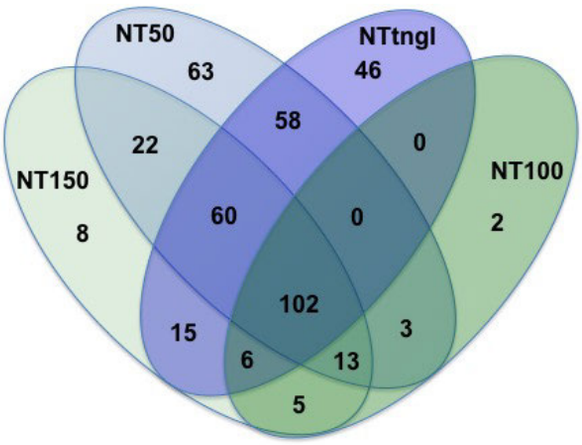
NT50
NTtngl
NT150
NT100
63
46
58
22
0
60
0
8
2
102
15
3
6
13
5

B

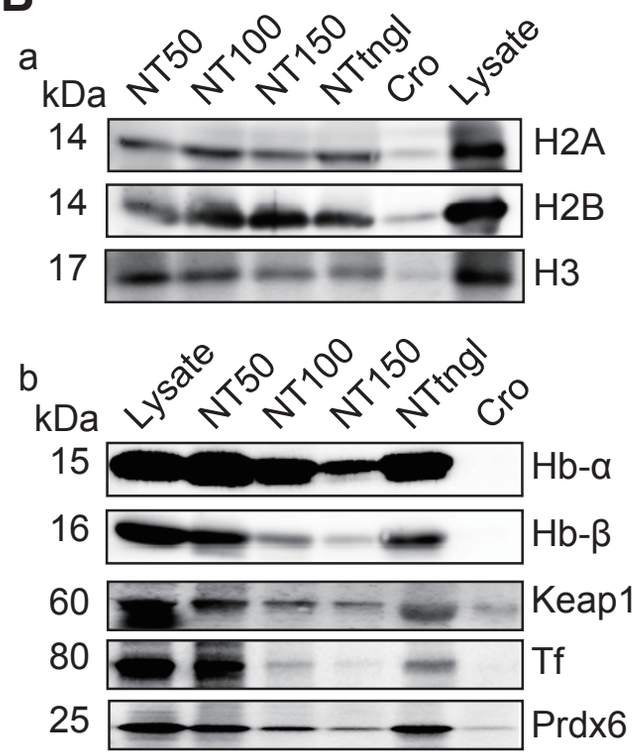
a
kDa
NT50
NT100
NT150
NTtngl
Cro
Lysate
14
H2A
14
H2B
17
H3
b
kDa
Lysate
NT50
NT100
NT150
NTtngl
Cro
15
Hb-α
16
Hb-β
60
Keap1
80
Tf
25
Prdx6

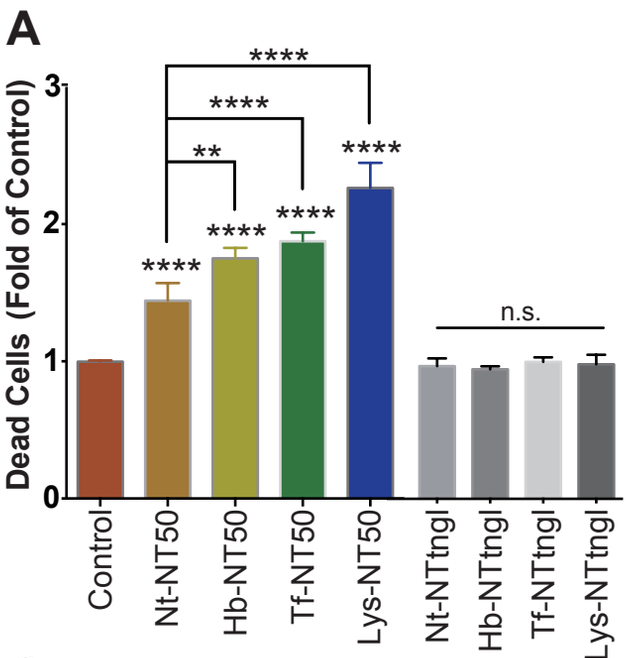
A
Dead Cells (Fold of Control)
0
1
2
3
****
****
**
****
****
****
n.s.
Control
Nt-NT50
Hb-NT50
Tf-NT50
Lys-NT50
Nt-NTtngl
Hb-NTtngl
Tf-NTtngl
Lys-NTtngl

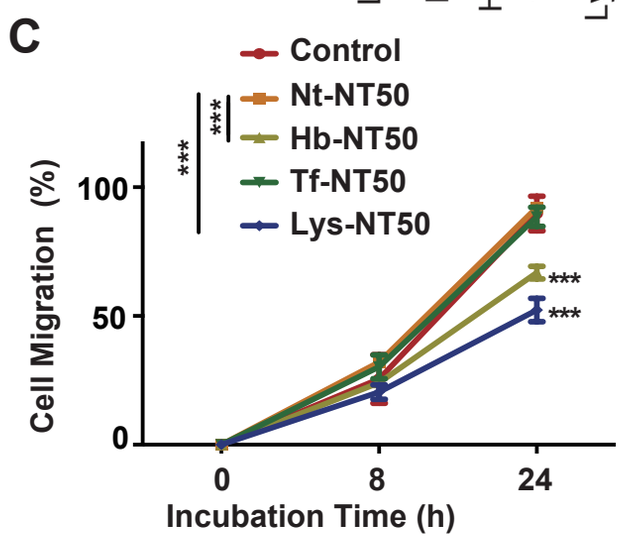
C
Control
Nt-NT50
Hb-NT50
Tf-NT50
Lys-NT50
***
***
***
***
Cell Migration (%)
0
50
100
0
8
24
Incubation Time (h)

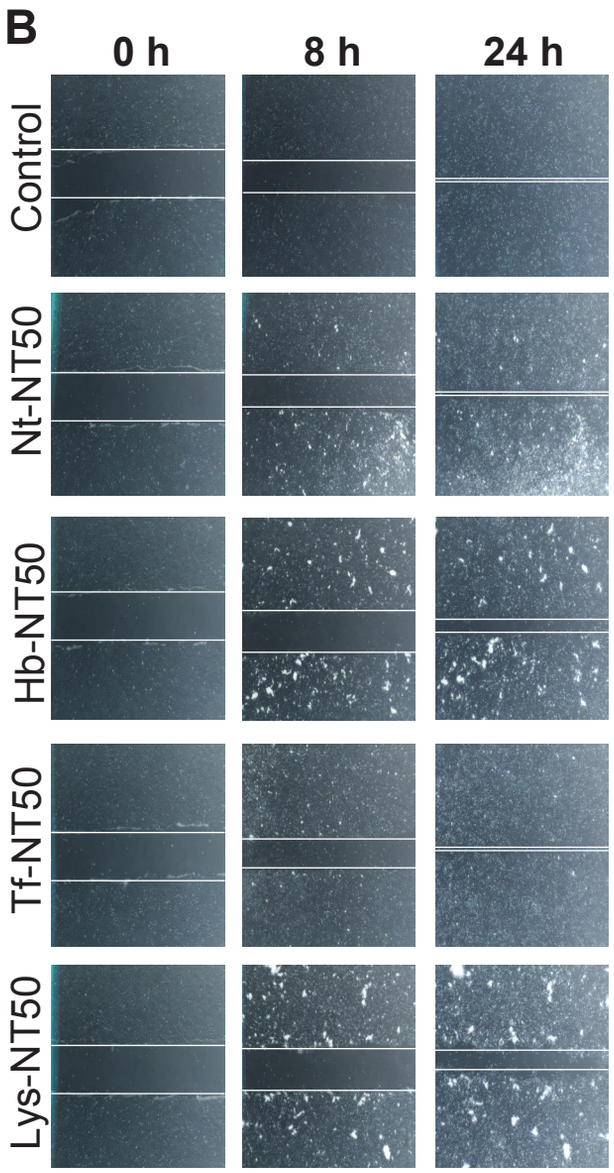
B
0 h
8 h
24 h
Control
Nt-NT50
Hb-NT50
Tf-NT50
Lys-NT50

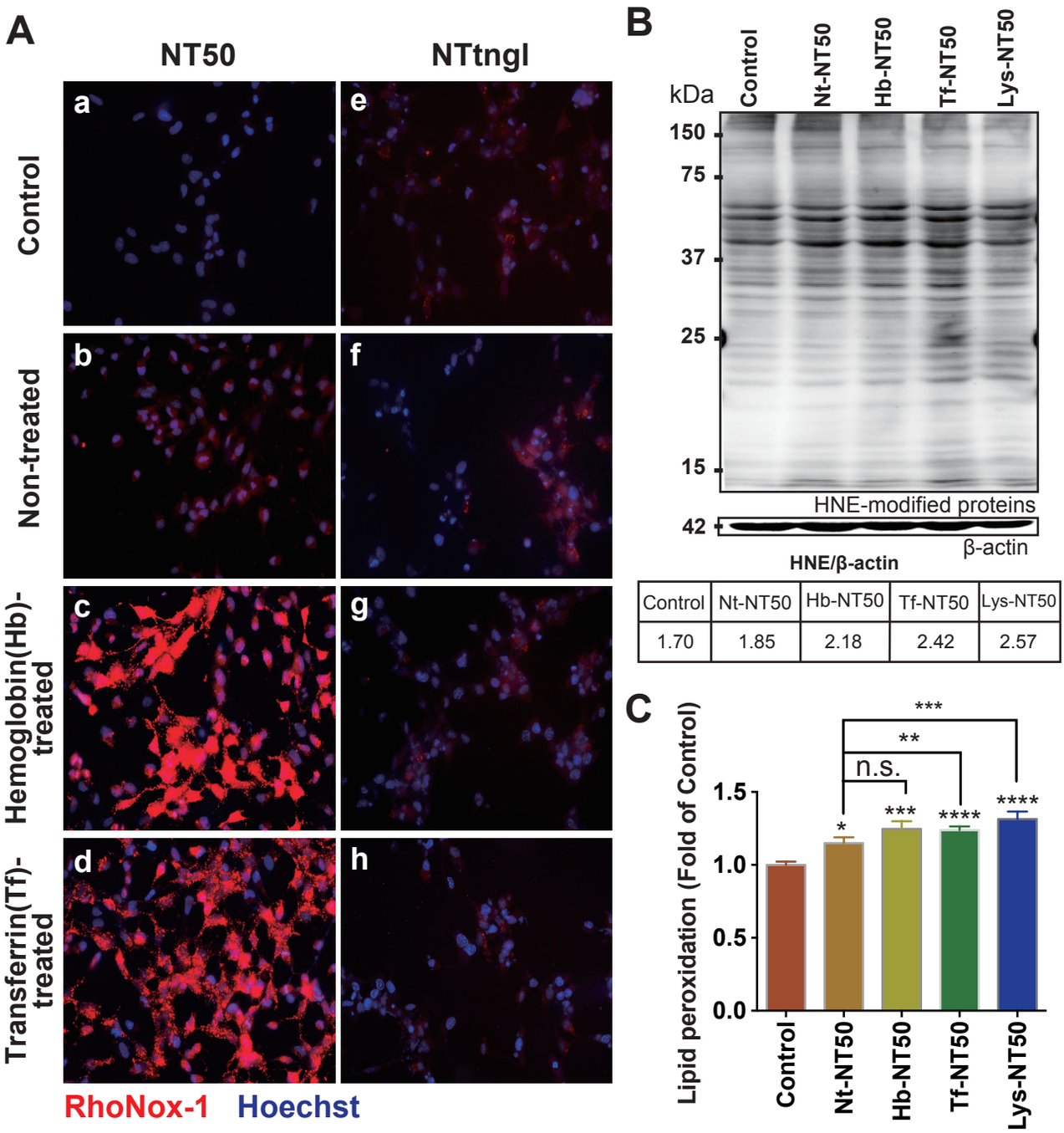

Control	Nt-NT50	Hb-NT50	Tf-NT50	Lys-NT50
1.70	1.85	2.18	2.42	2.57

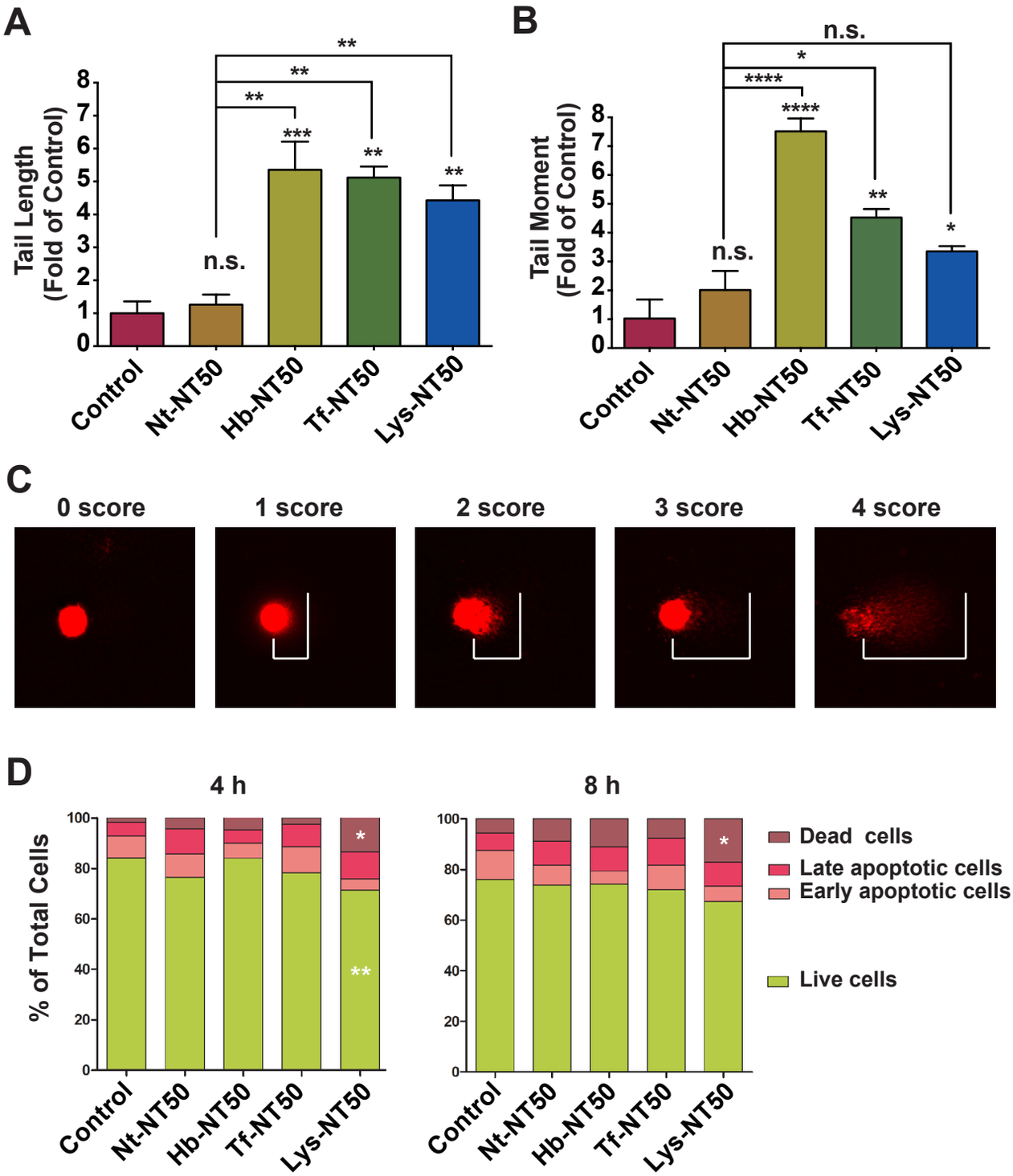
A
Tail Length
(Fold of Control)
n.s.
**
***
Control
Nt-NT50
Hb-NT50
Tf-NT50
Lys-NT50
B
Tail Moment
(Fold of Control)
n.s.
*
****
C
0 score
1 score
2 score
3 score
4 score
D
4 h
8 h
% of Total Cells
Dead cells
Late apoptotic cells
Early apoptotic cells
Live cells

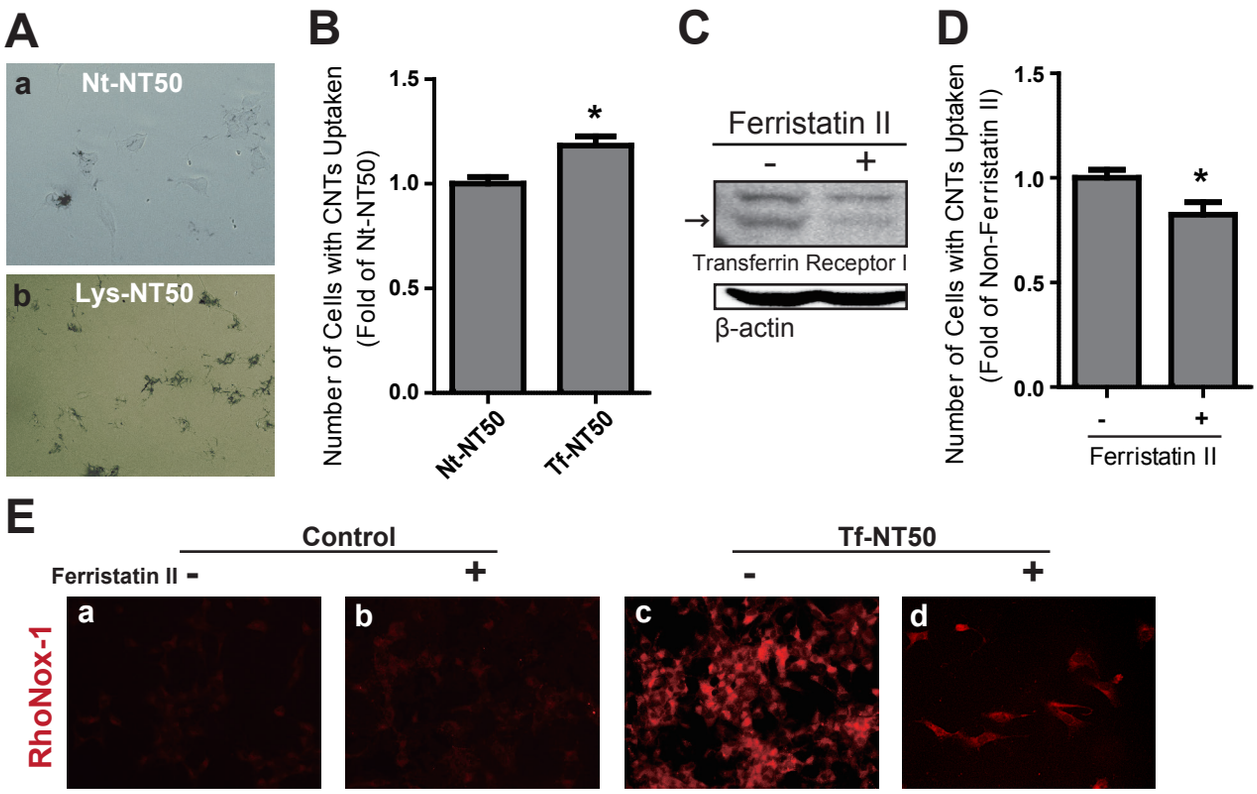
A
a
Nt-NT50
b
Lys-NT50
B
Number of Cells with CNTs Uptaken
(Fold of Nt-NT50)
1.5
1.0
0.5
0.0
*
Nt-NT50
Tf-NT50
C
Ferristatin II
-
+
Transferrin Receptor I
β-actin
D
Number of Cells with CNTs Uptaken
(Fold of Non-Ferristatin II)
1.5
1.0
0.5
0.0
*
-
+
Ferristatin II

E
Control
Tf-NT50
Ferristatin II -
+
-
+
RhoNox-1
a
b
c
d

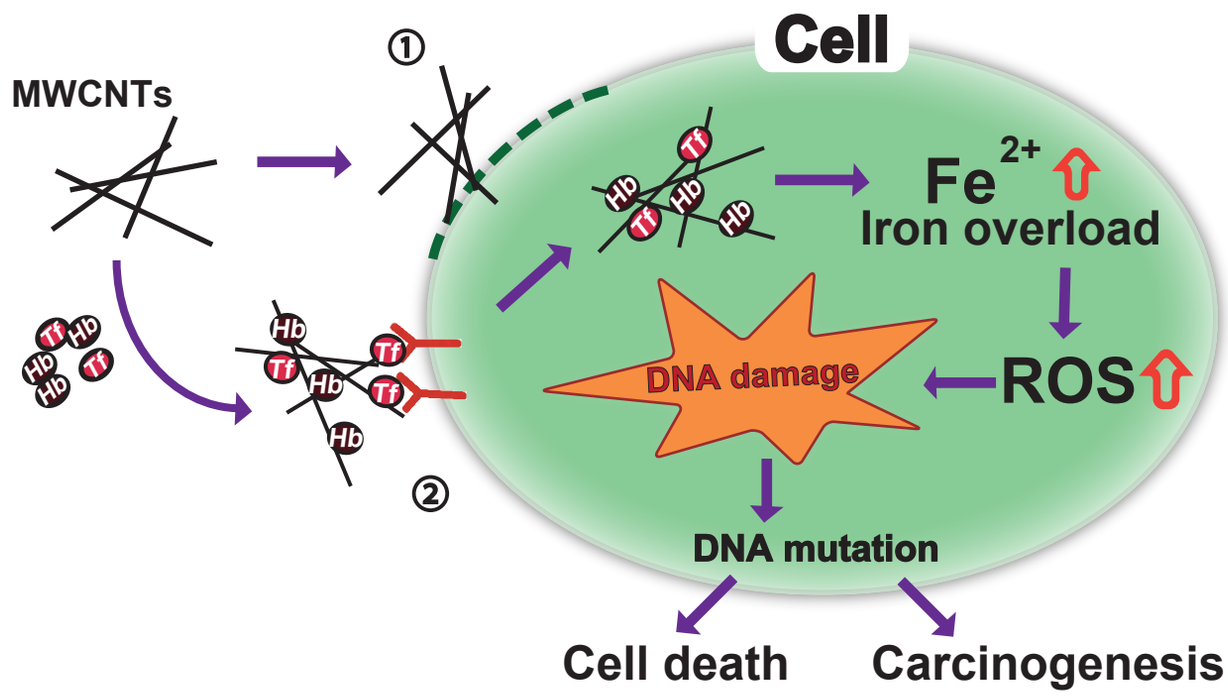

① Piercing ② Internalization with TfR1

Hb Hemoglobin Tf Transferrin Transferrin receptor 1

Table 1. A summarized result of In-solution digestion method

Accession	Mass	Original lysate	Biological role
VIME_RAT	53700	1,2,3,4	Vimentin
ALBU_RAT	68686	1,3,4	Serum albumin
ATPB_RAT	56318	1,3,4	ATP synthase subunit beta, mitochondrial
TRFE_RAT	76346	1,2,3,4	Serotransferrin
MOES_RAT	67697	1,2,3,4	Moesin
ACTB_RAT	41710	1,2,3,4	Actin, cytoplasmic 1
K1C19_RAT	44609	1,2,3,4	Keratin, type I cytoskeletal 19
A1I3_RAT	163670	1,3,4	Alpha-1-inhibitor 3
DESM_RAT	53424	1,2,3,4	Desmin
EHD2_RAT	61199	1,2,3,4	EH domain-containing protein 2
ATPA_RAT	59717	1,2,3,4	ATP synthase subunit alpha, mitochondrial
ACTA_RAT	41982	1,2,3,4	Actin, aortic smooth muscle
HSP7C_RAT	70827	1,2,3,4	Heat shock cognate 71 kDa protein
LMNA_RAT	74279	1,2,3,4	Prelamin-A/C
ACTC_RAT	41992	1,3,4	Actin, alpha cardiac muscle 1
MUG1_RAT	165221	4	Murinoglobulin-1
HBB1_RAT	15969	1,2,3,4	Hemoglobin subunit beta-1
TBB4B_RAT	49769	1,2,3,4	Tubulin beta-4B chain
K2C8_RAT	53985	1,2,3,4	Keratin, type II cytoskeletal 8
SPTN1_RAT	284462	1,4	Spectrin alpha chain, non-erythrocytic 1
TBA1B_RAT	50120	1,2,3,4	Tubulin alpha-1B chain
ENOA_RAT	47098	1,2,3,4	Alpha-enolase
TBA1A_RAT	50104	1,2,3,4	Tubulin alpha-1A chain
HBB2_RAT	15972	1,2,3,4	Hemoglobin subunit beta-2
K1C10_RAT	56470	1,2,3,4	Keratin, type I cytoskeletal 10
PTRF_RAT	43882	1,2,3,4	Polymerase I and transcript release factor
TBB2A_RAT	49875	1	Tubulin beta-2A chain
DPYL2_RAT	62239	1,2,3,4	Dihydropyrimidinase-related protein 2
TBB5_RAT	49639	1,2,3,4	Tubulin beta-5 chain
MYH9_RAT	226197	1,2,3,4	Myosin-9

1, NT50; 2, NT100; 3, NT150; 4, NTtngl. Refer to Table S2 for details.

Table 2. A summarized result of In-gel digestion method

Band No.	Accession	Mass	Protein Name
1	IQCAL_RAT	95,625	IQ and AAA domain-containing protein 1-like
2	KEAP1_RAT	69,399	Kelch-like ECH-associated protein 1
3	CP270_RAT	56,157	Cytochrome P450 2C70
4	MCM9_RAT	124,125	DNA helicase MCM9
5	DCAF8_RAT	66,156	DDB1- and CUL4-associated factor 8
6	SO4C1_RAT	78,648	Solute carrier organic anion transporter family member 4C1
7	NOS2_RAT	130,628	Nitric oxide synthase, inducible
8	ACTB_RAT	41,737	Actin, cytoplasmic 1
9	MOES_RAT	67,739	Moesin
10	TRFE_RAT	76,395	Serotransferrin
11	GBRP_RAT	50,481	Gamma-aminobutyric acid receptor subunit pi
12	SBP1_RAT	52,532	Selenium-binding protein 1
13	AL1A1_RAT	54,459	Retinal dehydrogenase 1
14	ALDH2_RAT	56,488	Aldehyde dehydrogenase, mitochondrial
15	FETA_RAT	68,386	Alpha-fetoprotein
16	H2A1C_RAT	14,105	Histone H2A type 1-C
17	H2A1F_RAT	14,176	Histone H2A type 1-F
18	H2AJ_RAT	14,045	Histone H2A.J
19	H2B1_RAT	13,990	Histone H2B type 1
20	H2B1A_RAT	14,225	Histone H2B type 1-A
21	H31_RAT	15,404	Histone H3.1
22	H4_RAT	11,367	Histone H4
23	RL23_RAT	14,865	60S ribosomal protein L23
24	RS16_RAT	16,445	40S ribosomal protein S16
25	RS14_RAT	16,259	40S ribosomal protein S14
26	HBA_RAT	15,329	Hemoglobin subunit alpha-1/2
27	HBB1_RAT	15,979	Hemoglobin subunit beta-1
28	HBB2_RAT	15,982	Hemoglobin subunit beta-2
29	ROA1_RAT	34,212	Heterogeneous nuclear ribonucleoprotein A1
30	ROA2_RAT	37,478	Heterogeneous nuclear ribonucleoproteins A2/B1
31	CAH2_RAT	29,114	Carbonic anhydrase 2

A

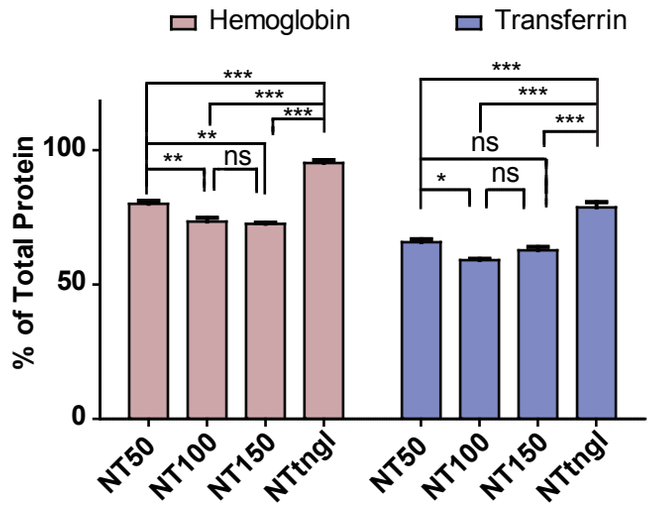

B

Surface Area (m^2/g)

NTtngl > NT50 > NT100 > NT150

Amount of Adsorbed Protein

NTtngl > NT50 > NT100 > NT150

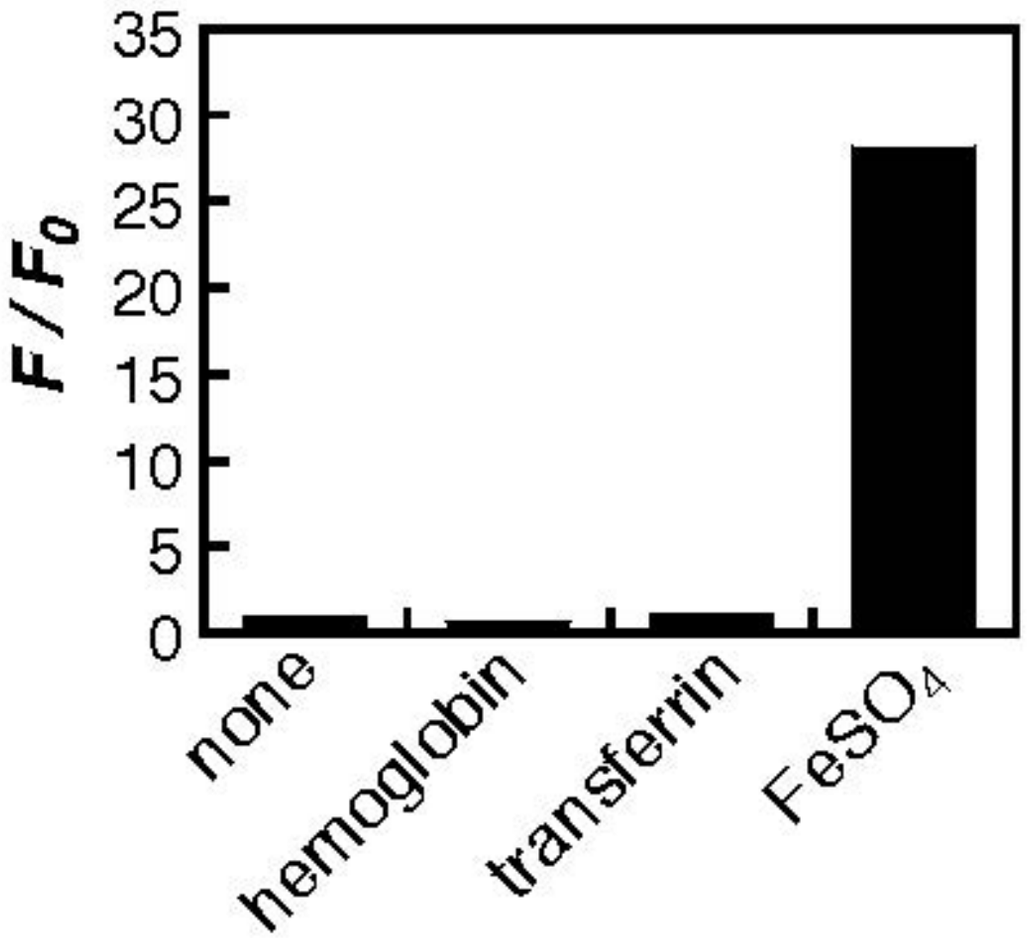
35
30
25
20
15
10
5
0
F / F0
none
hemoglobin
transferrin
FeSO4

Table S1. Overall summary table of characteristics of MWCNTs

Characteristic*	NT50a	NT50b	NT115	NT145	NTtngl
Manufacturer	Mitsui	Showa Denko	Showa Denko	Showa Denko	Showa Denko
Diameter by the company, nm	50	80	150	150	15
Diameter by authors, nm	49.95 ± 0.63	52.4 ± 0.72	116.2 ± 1.6	143.5 ± 1.6	ND
Length by the company, μm	4	10	8	6	3
Length by authors, μm	5.29 ± 0.12	4.6 ± 0.10	4.88 ± 0.10	4.34 ± 0.08	ND
Aggregation extent	High	High	Low	Low	Very high
G/D ratio	6.7 ± 0.34	9.5 ± 1.0	7.0 ± 0.6	5.5 ± 0.6	1.5 ± 0.1
ROS generation via EPR (S/M)	0.27 ± 0.01	0.14 ± 0.03	0.20 ± 0.07	0.13 ± 0.03	0.24 ± 0.01
Phagocytosis by macrophages	Yes	Yes	Yes	Yes	None
Toxicity to macrophages	Moderate	Moderate	Moderate	Moderate	Very low
Piercing mesothelial cell membrane	Yes	ND	Low	Very low	None
Toxicity to mesothelial cells	High	High	Low	Low	Low
Inflammogenicity to rats	High	ND	ND	Low	Low
Carcinogenicity to rats	High	High	ND	Low	None

Values presented as mean ± SEM where applicable. EPR, electron paramagnetic resonance; G/D, graphite/defect; ND, not determined; ROS, reactive oxygen species; S/M, signal to marker ratio.
*0.5 mg/mL in A-saline solution.

Table S2. The result of In-solution digestion method

Description	Accession	Original MWCNT	Mass (kDa)	Biological role
Thioredoxin	THIO_RAT	4	12	oxidoreductase
D-dopachrome decarboxylase	DOPD_RAT	1	13	catalytic enzyme
Profilin-1	PROF1_RAT	1,2,3,4	15	cytoskeleton
Transthyretin	TTHY_RAT	4	16	hormone binding
Coactosin-like protein	COTL1_RAT	4	16	cytoskeleton
Adenine phosphoribosyltransferase	APT_RAT	1,4	20	AMP formation
Protein DJ-1	PARK7_RAT	1,4	20	stress response
Alpha-crystallin B chain	CRYAB_RAT	3	20	stress response
Signal peptidase complex catalytic subunit SEC11A	SC11A_RAT	1,2,3	21	catalytic enzyme
Cysteine and glycine-rich protein 1	CSRP1_RAT	1,2,3	21	cell differentiation
Cell division control protein 42 homolog	CDC42_RAT	1,2,3,4	21	GTP/GDP binding
Ras-related C3 botulinum toxin substrate 1	RAC1_RAT	1,2,3,4	21	GTP/GDP binding
PRA1 family protein 3	PRAF3_RAT	3	22	protein regulation
Transforming protein RhoA	RHOA_RAT	1,4	22	GTP/GDP binding
Synaptosomal-associated protein 23	SNP23_RAT	4	23	protein regulator
Rho GDP-dissociation inhibitor 1	GDIR1_RAT	1,3,4	23	GDP/GTP regulation
C-type lectin domain family 2 member D11	CL2DB_RAT	3	24	antifungal immunity
Hypoxanthine-guanine phosphoribosyltransferase	HPRT_RAT	1	24	nucleotide binding
Protein-L-isoaspartate(D-aspartate) O-methyltransferase	PIMT_RAT	1	25	protein repair
Transmembrane emp24 domain-containing protein 10	TMEDA_RAT	1,3,4	25	protein transporter
Glutathione peroxidase 3	GPX3_RAT	3,4	25	stress response
GTP:AMP phosphotransferase AK3, mitochondrial	KAD3_RAT	1	25	catalytic enzyme
Anionic trypsin-1	TRY1_RAT	1	26	digestion
Triosephosphate isomerase	TPIS_RAT	1	27	catalytic enzyme
3-hydroxyacyl-CoA dehydrogenase type-2	HCD2_RAT	1,2	27	oxidoreductase
BPI fold-containing family A member 1	BPIA1_RAT	3,4	28	immune responses
Chloride intracellular channel protein 5	CLIC5_RAT	3,4	28	channel forming
Phosphoglycerate mutase 1	PGAM1_RAT	1,4	29	catalytic enzyme
Aquaporin-1	AQP1_RAT	3,4	29	formationof water channel
ATP synthase F(0) complex subunit B1, mitochondrial	AT5F1_RAT	1,4	29	ATP synthesis
NAD(P)H dehydrogenase [quinone] 1	NQO1_RAT	1	31	catalytic enzyme
Sodium/potassium-transporting ATPase subunit beta-3	AT1B3_RAT	1,3	32	catalytic enzyme
Corticosteroid 11-beta-dehydrogenase isozyme 1	DHI1_RAT	1,2,3	32	catalytic enzyme
Four and a half LIM domains protein 1	FHL1_RAT	1,2,3	32	protein regulator
Purine nucleoside phosphorylase	PNPH_RAT	1,2,3,4	32	catalytic enzyme
Beta-2-glycoprotein 1	APOH_RAT	1	33	glycoprotein binding
NADH-cytochrome b5 reductase 3	NB5R3_RAT	1,2,3,4	34	catalytic enzyme
60S acidic ribosomal protein P0	RLA0_RAT	1,2,3,4	34	DNA repair
rRNA 2'-O-methyltransferase fibrillarin	FBRL_RAT	1	34	catalytic enzyme
Mitochondrial 2-oxoglutarate/malate carrier protein	M2OM_RAT	2,3	34	catalytic enzyme
Hydroxyacyl-coenzyme A dehydrogenase, mitochondrial	HCDH_RAT	1,3	34	catalytic enzyme
Electron transfer flavoprotein subunit alpha, mitochondrial	ETFA_RAT	1,4	35	electron transporter
Myeloid-associated differentiation marker	MYADM_RAT	3,4	35	differentiation marker
Malate dehydrogenase, mitochondrial	MDHM_RAT	1,2,3,4	36	catalytic enzyme
Aldose reductase	ALDR_RAT	1	36	oxidoreductase
Glyceraldehyde-3-phosphate dehydrogenase	G3P_RAT	1,2,3,4	36	catalytic enzyme
Malate dehydrogenase, cytoplasmic	MDHC_RAT	1,3,4	36	catalytic enzyme
Class I histocompatibility antigen, Non-RT1.A alpha-1 chain	HA11_RAT	4	37	inflammatory response
3-alpha-hydroxysteroid dehydrogenase	DIDH_RAT	1	37	oxidoreductase
Transaldolase	TALDO_RAT	1,4	37	catalytic enzyme
Alpha-2-HS-glycoprotein	FETUA_RAT	1,4	38	inflammatory response
Lumican	LUM_RAT	4	38	cell shape
Haptoglobin	HPT_RAT	1,4	39	stress response
Fructose-bisphosphate aldolase A	ALDOA_RAT	1,3,4	39	catalytic enzyme
Phosphate carrier protein, mitochondrial	MPCP_RAT	2,3	39	protein transporter
Serum paraoxonase/lactonase 3	PON3_RAT	1,4	39	catalytic enzyme
Adenosine kinase	ADK_RAT	1	40	AMP formation
cAMP-dependent protein kinase catalytic subunit beta	KAPCB_RAT	1,3	41	ATP binding
Biglycan	PGS1_RAT	4	42	cell shape
RT1 class I histocompatibility antigen, AA alpha chain	HA12_RAT	1,3,4	42	inflammatory response
3-ketoacyl-CoA thiolase, mitochondrial	THIM_RAT	1	42	oxidoreductase
Endothelial cell-selective adhesion molecule	ESAM_RAT	1,4	42	cell shape
Alpha-parvin	PARVA_RAT	1,2,3,4	42	cytoskeleton
Alpha-centractin	ACTZ_RAT	1,4	43	ATP binding
Advanced glycosylation end product-specific receptor	RAGE_RAT	1,2,3,4	43	receptor
Creatine kinase B-type	KCRB_RAT	1,3,4	43	catalytic enzyme
Leukocyte elastase inhibitor A	ILEUA_RAT	1	43	protein regulator
Synaptic vesicle membrane protein VAT-1 homolog	VAT1_RAT	1,2,3,4	43	epidermal repair
Pyruvate dehydrogenase E1 component subunit alpha, somatic form, mitochondrial	ODPA_RAT	1	43	catalytic enzyme
Polymerase I and transcript release factor	PTRF_RAT	1,2,3,4	44	transcription
Neuroplastin	NPTN_RAT	4	44	cell adhesion
Lysosome-associated membrane glycoprotein 1	LAMP1_RAT	4	44	cell metastasis
Dynactin subunit 2	DCTN2_RAT	4	44	cell division
Phosphoglycerate kinase 1	PGK1_RAT	1,3,4	45	catalytic enzyme
Cathepsin D	CATD_RAT	3,4	45	endopeptidase
Acetyl-CoA acetyltransferase, mitochondrial	THIL_RAT	1,3	45	tricarboxylic acid cycle
Transmembrane protein 43	TMM43_RAT	3,4	45	nuclear envelope structure
Dipeptidase 1	DPEP1_RAT	1,2,3,4	45	catalytic enzyme
cAMP-dependent protein kinase type II-alpha regulatory subunit	KAP2_RAT	4	46	cAMP binding
SEC14-like protein 3	S14L3_RAT	1,2,3,4	46	hydrophobic ligands transporter
Alpha-1-antiproteinase	A1AT_RAT	1,3,4	46	inflammatory response
Serum deprivation-response protein	SDPR_RAT	3,4	46	phosphatidylserine binding
Eukaryotic initiation factor 4A-II	IF4A2_RAT	1,3,4	46	RNA helicase
Alpha-enolase	ENOA_RAT	1,2,3,4	47	glycolytic enzyme
Aspartate aminotransferase, mitochondrial	AATM_RAT	2,3,4	47	transaminase enzyme
Adenosylhomocysteinase	SAHH_RAT	1,3,4	48	methylcitric acid cycle
T-kininogen 1	KNT1_RAT	4	48	immune responses

Calreticulin	CALR_RAT	1,4	48	calcium ion binding
Equilibrative nucleoside transporter 1	S29A1_RAT	1,3	50	nucleoside transporter
Plasmalemma vesicle-associated protein	PLVAP_RAT	4	50	stomatal ormation
Fibulin-5	FBLN5_RAT	1,4	50	cell adhesion
Fibrinogen gamma chain	FIBG_RAT	1	51	platelet aggregation
Isocitrate dehydrogenase [NADP], mitochondrial	IDHP_RAT	1,3,4	51	oxidoreductase
Guanine deaminase	GUAD_RAT	1,2,3,4	51	hydrolase
Hemopexin	HEMO_RAT	1,4	51	heme transporter
Adenylyl cyclase-associated protein 1	CAP1_RAT	1,2,3,4	52	actin cytoskeleton organization
Citrate synthase, mitochondrial	CISY_RAT	1	52	catalytic enzyme
Selenium-binding protein 1	SBP1_RAT	1,4	52	protein transporter
6-phosphogluconate dehydrogenase, decarboxylating	6PGD_RAT	1,3	53	oxidoreductase
Desmin	DESM_RAT	1,2,3,4	53	gap junction
Vitamin D-binding protein	VTDB_RAT	4	54	vitamin transporter activity
Vimentin	VIME_RAT	1,2,3,4	54	cytoskeleton
Dihydrolipoyl dehydrogenase, mitochondrial	DLDH_RAT	1,4	54	oxidoreductase
Fatty aldehyde dehydrogenase	AL3A2_RAT	3,4	54	oxidoreductase
Retinal dehydrogenase 1	AL1A1_RAT	1,2,3,4	54	oxidoreductase
Plasma protease C1 inhibitor	IC1_RAT	4	56	immune responses
Cytosol aminopeptidase	AMPL_RAT	1,3	56	immune responses
Succinyl-CoA:3-ketoacid coenzyme A transferase 1, mitochondrial	SCOT1_RAT	1	56	catalytic enzyme
Carcinoembryonic antigen-related cell adhesion molecule 1	CEAM1_RAT	4	57	cell shape
Ectonucleoside triphosphate diphosphohydrolase 1	ENTP1_RAT	4	57	Hydrolase
Pyruvate kinase PKM	KPYM_RAT	1,2,3,4	58	catalytic enzyme
Tyrosine-protein kinase Lyn	LYN_RAT	1	59	immune responses
60 kDa heat shock protein, mitochondrial	CH60_RAT	1,3,4	61	Stress response
Glutamate dehydrogenase 1, mitochondrial	DHE3_RAT	1,2,3,4	61	oxidoreductase
Complement component receptor 1-like protein	CR1L_RAT	4	62	immune responses
Complement component C9	CO9_RAT	4	62	immune responses
Glucose-6-phosphate isomerase	G6PI_RAT	1,3,4	63	catalytic enzyme
WD repeat-containing protein 1	WDR1_RAT	1	66	cell junction
Lamin-B1	LMNB1_RAT	1,2,3,4	67	DNA repair
Calnexin	CALX_RAT	4	67	protein folding
Transketolase	TKT_RAT	1,3,4	68	catalytic enzyme
Moesin	MOES_RAT	1,2,3,4	68	Leukocyte migration
Serum albumin	ALBU_RAT	1,3,4	69	protein transporter
Phosphatidylinositol-binding clathrin assembly protein	PICAL_RAT	1	69	endocytosis
Ezrin	EZRI_RAT	1,2,3,4	69	cell shape
Kelch-like ECH-associated protein 1	KEAP1_RAT	1	69	stress response
Plastin-3	PLST_RAT	4	71	actin binding
78 kDa glucose-regulated protein	GRP78_RAT	1,3,4	72	stress response
Prelamin-A/C	LMNA_RAT	1,2,3,4	74	membrane formation
A-kinase anchor protein 5	AKAP5_RAT	4	76	cellular protein complex disassembly
Platelet endothelial cell adhesion molecule	PECA1_RAT	4	76	cell adhesion
Serotransferrin	TRFE_RAT	1,2,3,4	76	transporter
Nucleolin	NUCL_RAT	1,4	77	DNA-binding
Peroxisomal multifunctional enzyme type 2	DHB4_RAT	1	79	oxidoreductase
Junction plakoglobin	PLAK_RAT	1,2,3,4	82	cell adhesion
Niban-like protein 1	NIBL1_RAT	1	85	cell junction
Polymeric immunoglobulin receptor	PIGR_RAT	4	85	protein transporter
Membrane primary amine oxidase	AOC3_RAT	1,3,4	85	cell adhesion
Aconitate hydratase, mitochondrial	ACON_RAT	1,3	85	tricarboxylic acid cycle
Gelsolin	GELS_RAT	1,2,3,4	86	actin binding
Dipeptidyl peptidase 4	DPP4_RAT	1,2,3,4	88	cell adhesion
Transitional endoplasmic reticulum ATPase	TERA_RAT	1,3,4	89	DNA repair
Plasminogen	PLMN_RAT	2	90	fibrinolysis
Endoplasmin	ENPL_RAT	1,3,4	93	protein folding
Dynamin-2	DYN2_RAT	1	98	endocytosis
Alpha-actinin-1	ACTN1_RAT	1,4	103	cytoskeleton-associated
Band 3 anion transport protein	B3AT_RAT	1,3,4	103	anion transporter
Alpha-actinin-4	ACTN4_RAT	1,4	105	cytoskeleton-associated
Vinculin	VINC_RAT	2,3,4	117	cytoskeleton
Unconventional myosin-Ic	MYO1C_RAT	2,3,4	120	ATP binding
ATP-citrate synthase	ACLY_RAT	1	121	tricarboxylic acid cycle
Ceruloplasmin	CERU_RAT	3,4	121	oxidoreductase
Extended synaptotagmin-1	ESYT1_RAT	1	121	lipid transport
Xanthine dehydrogenase/oxidase	XDH_RAT	4	146	catalytic enzyme
Periaxin	PRAX_RAT	4	146	axon ensheathment
Alpha-1-inhibitor 3	A1I3_RAT	1,3,4	164	inflammatory response
Murinoglobulin-1	MUG1_RAT	4	165	inflammatory response
Alpha-1-macroglobulin	A1M_RAT	1,4	167	antiprotease
Complement C3	CO3_RAT	1,3,4	186	inflammatory response
Clathrin heavy chain 1	CLH1_RAT	3,4	191	protein transporter
Agrin	AGRIN_RAT	4	209	neuromuscular junction development
Spectrin beta chain, non-erythrocytic 2	SPTN2_RAT	1	271	actin-binding
Fatty acid synthase	FAS_RAT	1,3	272	oxidoreductase
Spectrin alpha chain, non-erythrocytic 1	SPTN1_RAT	1,4	284	actin-binding
Plectin	PLEC_RAT	1,4	533	actin-binding
14-3-3 protein				protein binding
14-3-3 protein beta/alpha	1433B_RAT	1,4	28	
14-3-3 protein epsilon	1433E_RAT	1,4	29	
14-3-3 protein eta	1433F_RAT	1,4	28	
14-3-3 protein gamma	1433G_RAT	1,4	28	
14-3-3 protein theta	1433T_RAT	1,4	28	
14-3-3 protein zeta/delta	1433Z_RAT	1,3,4	28	

40S ribosomal protein				translation
40S ribosomal protein S15a	RS15A_RAT	1,3	15	
40S ribosomal protein S2	RS2_RAT	2,3	31	
40S ribosomal protein S3	RS3_RAT	1,2,3,4	27	
40S ribosomal protein S4, X isoform	RS4X_RAT	2,3,4	30	
40S ribosomal protein S7	RS7_RAT	1,3,4	22	
40S ribosomal protein SA	RSSA_RAT	1,4	33	
60S ribosomal protein				translation
60S ribosomal protein L11	RL11_RAT	1,2	20	
60S ribosomal protein L23	RL23_RAT	1,2,3	15	
60S ribosomal protein L30	RL30_RAT	1	13	
60S ribosomal protein L5	RL5_RAT	1	34	
60S ribosomal protein L9	RL9_RAT	1	22	
Actin				Cytoskeleton-associated
Actin, alpha cardiac muscle 1	ACTC_RAT	1,3,4	42	
Actin, aortic smooth muscle	ACTA_RAT	1,2,3,4	42	
Actin, cytoplasmic 1	ACTB_RAT	1,2,3,4	42	
Actin, cytoplasmic 2	ACTG_RAT	1	42	
Actin-related protein 2	ARP2_RAT	1,4	45	
Actin-related protein 2/3 complex subunit 2	ARPC2_RAT	1,2,3	34	
Actin-related protein 3	ARP3_RAT	1	47	
ADP/ATP translocase				ATP/ADP transporter
ADP/ATP translocase 1	ADT1_RAT	1,2	33	
ADP/ATP translocase 2	ADT2_RAT	1,2,3,4	33	
ADP-ribosylation factor				protein transporter
ADP-ribosylation factor 1	ARF1_RAT	1,2,3,4	21	
ADP-ribosylation factor 3	ARF3_RAT	4	21	
ADP-ribosylation factor 4	ARF4_RAT	1,2,3,4	20	
ADP-ribosylation factor 5	ARF5_RAT	1,3,4	21	
ADP-ribosylation factor 6	ARF6_RAT	1,4	20	
ADP-ribosylation factor-like protein 8B	ARL8B_RAT	1,4	22	
Alcohol dehydrogenase				dehydrogenase enzymes
Alcohol dehydrogenase [NADP(+)]	AK1A1_RAT	1,4	36	
Aldehyde dehydrogenase, mitochondrial	ALDH2_RAT	1,3,4	56	
Annexin				Exocytosis
Annexin A1	ANXA1_RAT	1,2,3,4	39	
Annexin A2	ANXA2_RAT	1,2,3,4	39	
Annexin A3	ANXA3_RAT	1,3,4	36	
Annexin A4	ANXA4_RAT	1,3,4	36	
Annexin A5	ANXA5_RAT	1,2,3,4	36	
Annexin A6	ANXA6_RAT	1,3,4	76	
Annexin A8	ANXA8_RAT	1,4	37	
Apolipoprotein				lipid transporter
Apolipoprotein A-I	APOA1_RAT	4	30	
Apolipoprotein A-IV	APOA4_RAT	4	44	
Apolipoprotein E	APOE_RAT	4	36	
ATP synthase, mitochondrial				ATP synthesis
ATP synthase subunit alpha, mitochondrial	ATPA_RAT	1,2,3,4	60	
ATP synthase subunit beta, mitochondrial	ATPB_RAT	1,3,4	56	
ATP synthase subunit delta, mitochondrial	ATPD_RAT	4	18	
ATP synthase subunit gamma, mitochondrial	ATPG_RAT	1,2,3,4	30	
ATP synthase subunit O, mitochondrial	ATPO_RAT	1,2,3,4	23	
Calpain subunit				calcium ion binding
Calpain small subunit 1	CPNS1_RAT	1,3,4	29	
Calpain-2 catalytic subunit	CAN2_RAT	1	80	
Calponin				actin binding
Calponin-1	CNN1_RAT	1,3,4	33	
Calponin-3	CNN3_RAT	1	36	
Carbonic anhydrase				catalytic enzyme
Carbonic anhydrase 1	CAH1_RAT	1,2,3,4	28	
Carbonic anhydrase 2	CAH2_RAT	1,2,3,4	29	
Carbonic anhydrase 4	CAH4_RAT	1,3,4	35	
Carboxylesterase				detoxification
Carboxylesterase 1C	EST1C_RAT	4	60	
Carboxylesterase 1D	CES1D_RAT	1,3,4	62	
Caveolin				Stress response
Caveolin-1	CAV1_RAT	1,2,3,4	21	
Caveolin-2	CAV2_RAT	3,4	18	
CD				surface antigen
CD166 antigen	CD166_RAT	4	65	
CD59 glycoprotein	CD59_RAT	1,2,3,4	14	
Basal cell adhesion molecule	BCAM_RAT	1,3,4	67	
Intercellular adhesion molecule 1	ICAM1_RAT	4	60	
Junctional adhesion molecule A	JAM1_RAT	4	32	
Cell surface glycoprotein MUC18	MUC18_RAT	4	71	
Leukocyte surface antigen CD47	CD47_RAT	3,4	33	
CD81 antigen	CD81_RAT	3,4	26	
CD9 antigen	CD9_RAT	1,2,3,4	25	
Coronin				actin-binding
Coronin-1A	COR1A_RAT	1,3,4	51	
Coronin-1B	COR1B_RAT	1	54	
Cytochrome				oxidoreductase
Cytochrome b-c1 complex subunit 2, mitochondrial	QCR2_RAT	1,3,4	48	
Cytochrome c oxidase subunit 2	COX2_RAT	1,3,4	26	
Cytochrome c oxidase subunit 4 isoform 1, mitochondrial	COX41_RAT	1	20	
Cytochrome P450 2B1	CP2B1_RAT	1,2,3	56	
Cytochrome P450 4B1	CP4B1_RAT	1,2,3	59	

Dihydropyrimidinase-related protein				cell differentiation
Dihydropyrimidinase-related protein 2	DPYL2_RAT	1,2,3,4	62	
Dihydropyrimidinase-related protein 3	DPYL3_RAT	3	62	
Dimethylaniline monooxygenase [N-oxide-forming]				oxidoreductase
Dimethylaniline monooxygenase [N-oxide-forming] 1	FMO1_RAT	1,2,3,4	60	
Dimethylaniline monooxygenase [N-oxide-forming] 2	FMO2_RAT	1,2,3,4	61	
Dolichyl-diphosphooligosaccharide--protein glycosyltransferase				glycosyltransferase
Dolichyl-diphosphooligosaccharide--protein glycosyltransferase 48 kDa subunit	OST48_RAT	1,3	49	
Dolichyl-diphosphooligosaccharide--protein glycosyltransferase subunit 1	RPN1_RAT	1,4	68	
Dolichyl-diphosphooligosaccharide--protein glycosyltransferase subunit 2	RPN2_RAT	1,4	69	
EH domain-containing protein				ATP binding
EH domain-containing protein 2	EHD2_RAT	1,2,3,4	61	
EH domain-containing protein 3	EHD3_RAT	1,4	61	
Elongation factor				protein biosynthesis
Elongation factor 1-alpha 1	EF1A1_RAT	1,2,3,4	50	
Elongation factor 2	EF2_RAT	1,3,4	95	
Enoyl-CoA				fatty acid metabolism
Enoyl-CoA delta isomerase 1, mitochondrial	ECI1_RAT	1,4	32	
Enoyl-CoA hydratase, mitochondrial	ECHM_RAT	1	31	
F-actin-capping protein subunit				actin binding
F-actin-capping protein subunit alpha-1	CAZA1_RAT	1,4	33	
F-actin-capping protein subunit alpha-2	CAZA2_RAT	1,3,4	33	
F-actin-capping protein subunit beta	CAPZB_RAT	1	31	
Glutathione S-transferase				transferase
Glutathione S-transferase alpha-3	GSTA3_RAT	1,4	25	
Glutathione S-transferase alpha-4	GSTA4_RAT	1,4	25	
Glutathione S-transferase Mu 1	GSTM1_RAT	1,3	26	
Glutathione S-transferase Mu 2	GSTM2_RAT	1,2,3,4	26	
Glutathione S-transferase P	GSTP1_RAT	1,2,3,4	23	
Glutathione S-transferase Yb-3	GSTM4_RAT	1	26	
GTP-binding nuclear protein				chromatin binding
GTP-binding nuclear protein Ran	RAN_RAT	1,3,4	24	
GTP-binding nuclear protein Ran, testis-specific isoform	RANT_RAT	2	24	
Guanine nucleotide-binding protein				GTP binding
Guanine nucleotide-binding protein G(i) subunit alpha-2	GNAI2_RAT	1,2,3,4	40	
Guanine nucleotide-binding protein G(I)/G(S)/G(T) subunit beta-1	GBB1_RAT	1,3,4	37	
Guanine nucleotide-binding protein G(q) subunit alpha	GNAQ_RAT	1	42	
Guanine nucleotide-binding protein subunit beta-2-like 1	GBLP_RAT	1,3	35	
Heat shock protein				Stress response
Heat shock 70 kDa protein 1A/1B	HSP71_RAT	1,3,4	70	
Heat shock cognate 71 kDa protein	HSP7C_RAT	1,2,3,4	71	
Heat shock protein beta-1	HSPB1_RAT	1,2,3,4	23	
Heat shock protein HSP 90-alpha	HS90A_RAT	1,2,3,4	85	
Heat shock protein HSP 90-beta	HS90B_RAT	1,2,3,4	83	
Serpin H1	SERPH_RAT	1,3,4	46	
Hemoglobin subunit				Oxygen transporter
Hemoglobin subunit alpha-1/2	HBA_RAT	1,2,3,4	15	
Hemoglobin subunit beta-1	HBB1_RAT	1,2,3,4	16	
Hemoglobin subunit beta-2	HBB2_RAT	1,2,3,4	16	
Heterogeneous nuclear ribonucleoprotein				RNA binding
Heterogeneous nuclear ribonucleoprotein A1	ROA1_RAT	1	34	
Heterogeneous nuclear ribonucleoprotein A3	ROA3_RAT	1,2,3	40	
Heterogeneous nuclear ribonucleoprotein D0	HNRPD_RAT	1,3	38	
Heterogeneous nuclear ribonucleoprotein H	HNRH1_RAT	1	49	
Heterogeneous nuclear ribonucleoprotein H2	HNRH2_RAT	1,3	49	
Heterogeneous nuclear ribonucleoprotein K	HNRPK_RAT	1,3,4	51	
Heterogeneous nuclear ribonucleoprotein M	HNRPM_RAT	1,4	74	
Heterogeneous nuclear ribonucleoproteins A2/B1	ROA2_RAT	1,2,3,4	37	
Histone				Nucleosome assembly
Histone H1.1	H11_RAT	3	22	
Histone H1.4	H14_RAT	1,2,3,4	22	
Histone H2A	H2A1_RAT	1,3	14	
Histone H2A type 1-C	H2A1C_RAT	2,3,4	14	
Histone H2A type 2-A	H2A2A_RAT	1	14	
Histone H2A.Z	H2AZ_RAT	1,2,3,4	14	
Histone H2B	H2B1_RAT	1,2,3,4	14	
Core histone macro-H2A.1	H2AY_RAT	2,3,4	39	
Histone H3.1	H31_RAT	1,2,3	15	
Histone H3.3	H33_RAT	1,2,3,4	15	
Histone H4	H4_RAT	1,2,3,4	11	
Ig				antigen binding
Ig gamma-1 chain C region	IGHG1_RAT	1,4	36	
Ig gamma-2A chain C region	IGG2A_RAT	1,3,4	35	
Ig gamma-2B chain C region	IGG2B_RAT	1,4	36	
Ig gamma-2C chain C region	IGG2C_RAT	1	37	
Ig kappa chain C region, A allele	KACA_RAT	1,3,4	12	
Ig kappa chain C region, B allele	KACB_RAT	1,4	12	
Integrin				Signal transduction
Integrin alpha-1	ITA1_RAT	4	131	
Integrin beta-1	ITB1_RAT	1,4	88	
Integrin-linked protein kinase	ILK_RAT	1	51	
Keratin				Host-virus interaction
Keratin, type I cytoskeletal 10	K1C10_RAT	1,2,3,4	56	
Keratin, type I cytoskeletal 14	K1C14_RAT	1,2,3,4	53	
Keratin, type I cytoskeletal 15	K1C15_RAT	2,3	49	
Keratin, type I cytoskeletal 17	K1C17_RAT	1,3	48	
Keratin, type I cytoskeletal 18	K1C18_RAT	1,2,3,4	48	
Keratin, type I cytoskeletal 19	K1C19_RAT	1,2,3,4	45	
Keratin, type I cytoskeletal 4	K1C42_RAT	1,2,3,4	50	
Keratin, type II cytoskeletal 1	K2C1_RAT	1,2,3,4	65	

Keratin, type II cytoskeletal 2 epidermal	K22E_RAT	1,2,3,4	69	
Keratin, type II cytoskeletal 4	K2C4_RAT	4	58	
Keratin, type II cytoskeletal 5	K2C5_RAT	1,2,3,4	62	
Keratin, type II cytoskeletal 6A	K2C6A_RAT	1,2,3,4	59	
Keratin, type II cytoskeletal 7	K2C7_RAT	1,2,3,4	51	
Keratin, type II cytoskeletal 72	K2C72_RAT	1,2,3,4	57	
Keratin, type II cytoskeletal 73	K2C73_RAT	1,2,3,4	60	
Keratin, type II cytoskeletal 75	K2C75_RAT	2,3	59	
Keratin, type II cytoskeletal 8	K2C8_RAT	1,2,3,4	54	
L-lactate dehydrogenase chain				catalytic enzyme
L-lactate dehydrogenase A chain	LDHA_RAT	1,2,3,4	36	
L-lactate dehydrogenase B chain	LDHB_RAT	1,3,4	37	
Myosin				cell motility
Myosin light polypeptide 6	MYL6_RAT	4	17	
Myosin-10	MYH10_RAT	1,2,3,4	229	
Myosin-11 (Fragments)	MYH11_RAT	1,2,3,4	152	
Myosin-6	MYH6_RAT	1,2,3	223	
Myosin-7	MYH7_RAT	1,3	223	
Myosin-9	MYH9_RAT	1,2,3,4	226	
Nucleoside diphosphate kinase				catalytic enzyme
Nucleoside diphosphate kinase A	NDKA_RAT	1	17	
Nucleoside diphosphate kinase B	NDKB_RAT	1,3,4	17	
Peptidyl-prolyl cis-trans isomerase				Protein folding
Peptidyl-prolyl cis-trans isomerase A	PPIA_RAT	1,2,3,4	18	
Peptidyl-prolyl cis-trans isomerase B	PPIB_RAT	1,2,3,4	24	
Peroxiredoxin				Oxidoreductase
Peroxiredoxin-1	PRDX1_RAT	1,4	22	
Peroxiredoxin-2	PRDX2_RAT	1,4	22	
Peroxiredoxin-5, mitochondrial	PRDX5_RAT	1	22	
Peroxiredoxin-6	PRDX6_RAT	1,2,3,4	25	
Polypyrimidine tract-binding protein				RNA binding
Polypyrimidine tract-binding protein 1	PTBP1_RAT	1,3,4	59	
Polypyrimidine tract-binding protein 3	PTBP3_RAT	1	57	
Prohibitin				DNA synthesis inhibitor
Prohibitin	PHB_RAT	1,3,4	30	
Prohibitin-2	PHB2_RAT	1,2,3,4	33	
Proteasome subunit				peptide binding
Proteasome subunit alpha type-2	PSA2_RAT	1,3,4	26	
Proteasome subunit alpha type-5	PSA5_RAT	4	26	
Proteasome subunit alpha type-6	PSA6_RAT	1	27	
Proteasome subunit alpha type-7	PSA7_RAT	1,4	28	
Proteasome subunit beta type-1	PSB1_RAT	1	26	
Proteasome subunit beta type-2	PSB2_RAT	1	23	
Proteasome subunit beta type-3	PSB3_RAT	1,3	23	
Proteasome subunit beta type-4	PSB4_RAT	1	29	
Protein disulfide-isomerase				catalytic enzyme
Protein disulfide-isomerase	PDIA1_RAT	4	57	
Protein disulfide-isomerase A3	PDIA3_RAT	1,4	57	
Protein disulfide-isomerase A6	PDIA6_RAT	1,4	48	
Pulmonary surfactant-associated protein				respiration
Pulmonary surfactant-associated protein A	SFTPA_RAT	4	26	
Pulmonary surfactant-associated protein B	PSPB_RAT	1,4	42	
Rab GDP dissociation inhibitor				GTP/GDP regulation
Rab GDP dissociation inhibitor alpha	GDIA_RAT	1,3,4	51	
Rab GDP dissociation inhibitor beta	GDIB_RAT	1,3,4	51	
Ras-related protein				GTP/GDP binding
Ras-related protein Rab-10	RAB10_RAT	1	23	
Ras-related protein Rab-11B	RB11B_RAT	1,2,3,4	24	
Ras-related protein Rab-14	RAB14_RAT	1,2,3,4	24	
Ras-related protein Rab-1A	RAB1A_RAT	1,2,3,4	23	
Ras-related protein Rab-1B	RAB1B_RAT	1,2,3,4	22	
Ras-related protein Rab-2A	RAB2A_RAT	1,3,4	24	
Ras-related protein Rab-35	RAB35_RAT	3,4	23	
Ras-related protein Rab-6A	RAB6A_RAT	1,2,3,4	24	
Ras-related protein Rab-7a	RAB7A_RAT	1,4	23	
Ras-related protein Rab-8A	RAB8A_RAT	1	24	
Ras-related protein Rab-8B	RAB8B_RAT	3	24	
Ras-related protein Ral-A	RALA_RAT	1	24	
Ras-related protein Ral-B	RALB_RAT	1,3,4	23	
Ras-related protein Rap-1A	RAP1A_RAT	1,2,3,4	21	
Ras-related protein Rap-1b	RAP1B_RAT	1,2,3,4	21	
Ras-related protein R-Ras	RRAS_RAT	1	24	
Reticulon				membrane trafficking
Reticulon-3	RTN3_RAT	3	101	
Reticulon-4	RTN4_RAT	3	126	
Septin				GTP binding
Septin-11	SEP11_RAT	1	50	
Septin-2	SEPT2_RAT	1,4	42	
Septin-7	SEPT7_RAT	1,3,4	50	
Serine protease inhibitor				protease inhibitor
Serine protease inhibitor A3K	SPA3K_RAT	1,4	47	
Serine protease inhibitor A3L	SPA3L_RAT	1,3,4	46	
Serine protease inhibitor A3M (Fragment)	SPA3M_RAT	4	46	
Serine protease inhibitor A3N	SPA3N_RAT	1,4	47	
Serine/threonine-protein phosphatase PP1-beta catalytic subunit	PP1B_RAT	1	37	
T-complex protein 1 subunit				protein folding
T-complex protein 1 subunit beta	TCPB_RAT	1,4	57	
T-complex protein 1 subunit gamma	TCPG_RAT	1	61	

Transgelin				Actin cross-linking/gelling protein
Transgelin	TAGL_RAT	1,3,4	23	
Transgelin-2	TAGL2_RAT	1	22	
Trifunctional enzyme subunit, mitochondrial				catalytic enzyme
Trifunctional enzyme subunit alpha, mitochondrial	ECHA_RAT	1,3	83	
Trifunctional enzyme subunit beta, mitochondrial	ECHB_RAT	1,2,3	51	
Tubulin				GTP binding
Tubulin alpha-1A chain	TBA1A_RAT	1,2,3,4	50	
Tubulin alpha-1B chain	TBA1B_RAT	1,2,3,4	50	
Tubulin beta-2A chain	TBB2A_RAT	1	50	
Tubulin beta-4B chain	TBB4B_RAT	1,2,3,4	50	
Tubulin beta-5 chain	TBB5_RAT	1,2,3,4	50	
Ubiquitin				structural constituent of ribosome
Ubiquitin-40S ribosomal protein S27a	RS27A_RAT	1,2,3	18	
Ubiquitin-60S ribosomal protein L40	RL40_RAT	4	15	
Ubiquitin-like modifier-activating enzyme 1	UBA1_RAT	1	118	
Vesicle				SNAP receptor
Vesicle-associated membrane protein 2	VAMP2_RAT	1,4	13	
Vesicle-trafficking protein SEC22b	SC22B_RAT	1,3	25	
Voltage-dependent anion-selective channel protein				channel forming
Voltage-dependent anion-selective channel protein 3	VDAC1_RAT	1,2,3,4	31	
Voltage-dependent anion-selective channel protein 2	VDAC2_RAT	1,2,3,4	32	
Voltage-dependent anion-selective channel protein 3	VDAC3_RAT	1,3	31	

1, NT50; 2, NT100; 3, NT150; 4, NTtngl